Journal of Power Sources 240 (2013) 558–582

Contents lists available at SciVerse ScienceDirect

Journal of Power Sources

journal homepage: www.elsevier.com/locate/jpowsour

Review

# Degradation aspects of water formation and transport in Proton Exchange Membrane Fuel Cell: A review

T. Ous*, C. Arcoumanis

*School of Engineering and Mathematical Sciences, City University London, Northampton Square, London EC1V 0HB, United Kingdom*

## HIGHLIGHTS

- The effect of water formation and transport on PEMFC durability varies with cell's designs.
- The effect of water accumulation on PEMFC durability is detrimental at sub-freezing temperatures.
- The impact of water mechanisms on PEMFC durability can be classified as ageing or catastrophic.

## ARTICLE INFO

*Article history:*
Received 23 July 2012
Received in revised form
11 January 2013
Accepted 7 April 2013
Available online 16 May 2013

*Keywords:*
PEMFC
Water management
Degradation
Water formation and transport
Flooding
Ice formation

## ABSTRACT

This review paper summarises the key aspects of Proton Exchange Membrane Fuel Cell (PEMFC) degradation that are associated with water formation, retention, accumulation, and transport mechanisms within the cell. Issues related to loss of active surface area of the catalyst, ionomer dissolution, membrane swelling, ice formation, corrosion, and contamination are also addressed and discussed. The impact of each of these water mechanisms on cell performance and durability was found to be different and to vary according to the design of the cell and its operating conditions. Overall, the impact of water mechanisms can be classified as aging or catastrophic. Ageing has a long-term impact over the duration of the PEMFC life-time whereas in the catastrophic mechanism the impact is immediate. The conversion of cell residual water into ice at sub-freezing temperatures by the water retention/accumulation mechanism and the access of poisoning contaminants through the water transport mechanism are considered to fall into the catastrophic category. The effect of water mechanisms on PEMFC degradation can be reduced or even eliminated by (a) using advanced materials for improving the electrical, chemical and mechanical stability of the cell components against deterioration, and (b) implementing effective strategies for water management in the cell.



## 1. Introduction

Fuel cells have the potential to resolve the current energy crisis of the 21st century. These electrochemical energy devices convert the chemical energy of hydrogen fuel into electrical energy efficiently [1]. They offer great flexibility in their design which allows them to be in various configurations and to operate with a wide range of hydrocarbon fuels, features that broaden the scope of their applications. Furthermore, the fact that hydrogen is an abundant source gives fuel cells the advantage to be one of the most sustainable solutions for future energy needs.

The commercialisation of fuel cells is mainly affected by their high cost and the lack of a hydrogen infrastructure. Attempts to reduce the cost of fuel cells and to develop a global hydrogen network for their use are still ongoing. The primary focus is to minimise the loading of Platinum (Pt) in the catalyst of the Membrane Electrode Assembly (MEA) which is considered to be the main contributor to the high cost [2]. Some studies have suggested the use of more effective techniques for Pt deposition onto the catalyst to reduce its loading [3–7], others concentrated on enhancing the polarisation performance of the cell to compensate for further Pt reduction [8–10]. Although some studies [11] claimed that reduction of up to 50% (e.g. 0.15 mg-Pt $cm^{-2}$) is achievable with marginal compromise to the fuel cell stack efficiency (<1%), further reduction is still needed [12]. The manufacturing cost of fuel cell components, particularly the MEA and the Gas Diffusion Layer (GDL), is another significant contributor to the overall cost [2]. An approach which can make them more affordable is to increase the manufacturing volume of fuel cell stacks and to reduce the complexity of the manufacturing processes of some of their

* Corresponding author.
*E-mail addresses:* t.ous@city.ac.uk (T. Ous), C.Arcoumanis@city.c.uk (C. Arcoumanis).

0378-7753/$ – see front matter © 2013 Elsevier B.V. All rights reserved.
http://dx.doi.org/10.1016/j.jpowsour.2013.04.044

components [2]. It is expected that, as fuel cell stacks become commercially viable, hydrogen fuelling infrastructure will be established that is easily accessible for supporting the penetration of fuel cells into the market place [13,14]. This remains a major concern particularly for the transport sector where issues associated with hydrogen production [15,16], safety [17–19], on-board and off-board storage [20–22] have surfaced.

The durability of fuel cells is another obstacle affecting their commercialisation [23]. Currently, PEMFCs can operate for some 2500 h in transportation [24]. Although this timescale has doubled in recent years, it is still inadequate and may need further doubling (~5000 h) in order to meet the target for year 2015 aimed by the US Department of Energy (DOE), the Japan's New Energy and Industrial Technology Development Organisation (NEDO), and the European Hydrogen and Fuel Cell Technology Platform (HFP). For stationary applications, the life-time requirement for fuel cells extends to 40,000 h [25]. The reason for the longer life period in this case is attributed to the fact that the fuel cell load is more stable than under transport conditions. The rapid change in fuel cell load, usually referred to as dynamic load cycling, affects significantly the degradation rate [26] and the life-time expectancy of the cell [27]. Potential load cycling can severely affect the mechanical and chemical properties of the catalyst and its carbon support leading to an early cell failure [28].

Various durability tests were implemented by fuel cell developers in order to predict their life-time under practical operating conditions. Emphasis on developing accelerated life-time tests, also called accelerated stress tests (ASTs), has increased in recent years to prevent the prolonged test periods and high costs associated with real time tests. The results obtained from those accelerated tests were found not to be consistent and to differ considerably from the real lifetime or steady state measurements [28–34]. This is probably expected as measurements were carried out under different operating conditions and for different fuel cell component designs. Furthermore, some durability measurements [35–42] were made of individual components rather than of the complete cell unit. Thus, the effect of degradation on the neighbouring components which consequently affects the life-time of the entire cell will not be represented. This stresses the need for standardised durability protocols which would ensure uniformity between these measurements.

Degradation of PEMFC can be caused by a number of factors associated with the design of the cell and its operation. These factors can be classified into two types: catastrophic and ageing. Catastrophic factors are the ones that can cause immediate or early failure in cell performance due to severe mechanical or chemical damage to the cell during operation. The Pinhole formation on the surface of the membrane, for instance, can be very damaging to the cell since it allows reactant gases to cross-over from the anode or the cathode side leading to catalytic combustion and a sudden drop in the cell's power output [43,44]. Membrane perforations or cracks in the cell components may be the result of impaired design/fabrication during preparation process, improper cell assembly, or operation of the cell at extremely high pressures and temperatures. Membrane poisoning is another detrimental factor to the lifetime of PEMFC. High concentration levels of impurities such as carbon monoxide (CO) in the reactant gases results in CO adsorption to the platinum surface of the catalyst which blocks the active hydrogen sites [45,46].

Ageing factors represent the natural cause of degradation due to cell electrochemical reaction. Unlike catastrophic, their effects on depleting cell's performance occur gradually. Three phases of voltage drop were identified in the ageing process representing stable operation, slow decrease in cell voltage and rapid fall in voltage [47]. The degradation rate is a function of the operational time of the cell and is usually expressed as the drop in microvolt scale per hour of operation (e.g. $\mu V\ hr^{-1}$). This rate is strongly dependant on the deterioration rate of the cell's materials such as the change in the mechanical and chemical properties of the catalyst including the loss in electro-catalyst surface area due to growth in the platinum particle size [48,49], corrosion of platinum-based catalysts [50,51], and corrosion of carbon support catalyst [52]. A comprehensive review of PEMFC components degradation can be found in Ref. [53].

Although deterioration of the material is inevitable, due to the electrochemical nature of the fuel cell reaction, its rate can be minimised. Many attempts were made in the past few years to develop more robust components and operational regimes capable of withstanding harsh fuel cell conditions against degradation. In Ref. [54] the design of membranes was suggested to be made thicker to reduce hydrogen crossover to the cathode. According to Ref. [55], sulfonated polymide membranes exhibit better stability than Nafion under electric load cycling. Refs. [56,57] found Pt stability in the catalyst to be improved against dissolution by using multiwalled carbon nanotubes (CNTs) and by modifying Pt nanoparticles with gold (Au) clusters. Others [58,59] have pointed to the effect of carbon film coating on improving the mechanical and electrical properties of gas diffusion layers. In Ref. [60] the role of homogeneous coating in controlling the diffusion overvoltage from the gas diffusion layers was revealed. Several other studies [61–66] stressed the importance of coating for bipolar plates to prevent surface corrosion. Refs. [67,68] suggested to operate PEMFC under low relative humidity (RH) to minimise the loss of Pt active surface area contrary to Refs, [48,69] which concluded that low RH increases carbon corrosion in the catalyst. Others like Ref. [44] suggested reducing RH, temperature and hydrogen pressure during PEMFC operation to suppress the hydrogen cross-over mechanism. The influence of fuel and oxidant starvation [70], open circuit operation [71], excessive air bleeding [72], humidity cycling [73,74], load-on/off cycling [75], and freeze/thaw cycling [76] on structural changes of the membrane was also demonstrated. A more detailed analysis of the effect of the operating conditions on the PEMFC durability can be found in Ref. [77].

Despite all these investigations, very few studies have highlighted the role of water on the degradation of PEMFC. This review paper attempts to focus on the impact of (a) water production during the electrochemical reaction of the cell, (b) water accumulation in the channels and reaction sites and (c) water transport mechanisms on the electrical, mechanical, thermal and chemical/electrochemical deterioration of the PEMFC components.

## 2. Water distribution and transport

Good water distribution in PEMFC is a recipe for achieving effective water management and enhanced performance of the cell [218]. The ionic conductivity of Nafion is strongly dependant upon the amount of water available in the membrane [78]. The water which is absorbed by the sulphonic acid groups (HSO3) of the membrane due to its hydrophilic characteristic enables $H^+$ ions to move freely on weakening the attraction force between $H^+$ and $SO_3^-$ ions [79]. The more water molecules are present in each $SO_3^-$ chain, the better the conductivity of $H^+$ becomes. Nevertheless, too much water can block the reaction sites of the neighbouring electrodes preventing the access of reactant gases to the cell. Therefore, the amount of water in these two regions must be kept in optimum balance for cell performance.

New materials and designs were developed to maintain this delicate balance. Appropriate loading of oxygen permeable and hydrophobic dimethyl silicone oil (DSO) [80], hygroscopic γ-alumina particles [81], silicon dioxide particles [82,83] and silica-

based composites [84,85] on the catalyst layer showed improvement in the wettability of the membrane under low humidification conditions. Chao et al. [81] revealed that the addition of only 10% of γ-alumina to the anode catalyst layer is sufficient to increase the wettability and achieve high cell performance. Although with addition of 40% of γ-alumina the wettability increased, which was evident from the decrease in the droplets contact angle with the catalyst surface (109° at 10% and 0° at 40% loading), the polarisation performance of the cell dropped due to flooding. Similar drop in performance, because of flooding, was reported in Jung et al. [83] when $SiO_2$ was loaded to the cathode catalyst layer; they found that loading the anode with 40 wt.% of $SiO_2$ gives the best performance even under 0% relative humidity of the anode.

The use of a micro porous layer (MPL) between the gas diffusion and catalyst layers proved to offer advantages towards flooding in PEMFC. Generally, the water saturates at the interface of the catalyst with GDL [86] due to a sudden change in the pore size of these mated layers [87]. As a result, a water film is formed at the interface region where more space is available to accommodate the accumulated water. To some extent, MPL acts as a barrier limiting the access of water flow to the GDL [88] while facilitating an effective water drainage mechanism [89]. When Yau et al. [88] inserted MPL into the MEA design, the back diffusion of water to the anode was enhanced. Eventually, the water cross-over flux from the cathode to the anode was increased (e.g. 33.7% with MPL versus 27.4% without MPL at $RH_c = 26\%$ and $RH_a = 75\%$ respectively) indicating less passage of water to the GDL micro-channels.

Coating MPL with hydrophobic substances such as fluorinated ethylene propylene (FEP) [90], polytetrafluoroethylene (PTFE) [91,92], or with copolymer containing hydrophilic functional groups [93] and composite carbon black [94], has been suggested as an effective strategy for managing water transport within the cell. The improvement in cell polarisation [90] was clearly due to the change in FEP loading (e.g. 30% FEP loading by screen-printed technique) which served to expel excessive product water. The increase in PTFE and carbon loading tends to reduce water diffusion into the GDL channels [91,95]. When the PTFE loading on MPL increased from 0 to 40 wt.%, the water flux across the GDL was reduced by almost 30% under an air flow rate of 4SLPM (0.75 g $min^{-1}$ to 0.55 g $min^{-1}$) [91]. Furthermore, increasing the amount of PTFE in the MPLs makes the in-plane permeability within the GDL higher [92]. Different carbon materials for MPL were examined including acetylene black, composite carbon black (80 wt.% acetylene black + 20 wt.% black pearls 2000) and black pearls 2000 [94]. The cell with the composite carbon material exhibited the best performance. Their polarisation measurements were supported by Scanning Electron Microscopy (SEM) observation of MPL structure. The images showed formation of bi-functional pores on the surface which facilitated the transport of both reactants and liquid water.

Similarly, the change of MPL morphology with respect to the pore size diameter, layer thickness [96] and surface roughness [97] has an effect on water mass transfer and local transport. In Ref. [97] the importance of MPL surface roughness towards water transport at the interfacial region of MPL/catalyst (CL) was highlighted. The role of surface roughness becomes more pronounced under compressive conditions where interfacial gabs and macro-cracks can be formed. Their optical profilometry measurements revealed that cracks on the MPL surface occur at random locations and in various magnitudes to the extent that they can be as deep as the entire thickness of the MPL. Fig. 1 shows a cross-sectional SEM image of a cracked MPL where a large-size channel was created across the layer enabling easy passage for the water flow.

Under low humidification conditions when maintaining full hydration of the membrane is arduous, the size of MPL pores is kept minimal in order to restrict the flow of by-product water to GDL and avoid drying up the membrane [98]. Kitahara et al. [98] were able to improve cell performance under 0% RH of reactant air when they reduced the mean pore diameter of MPL from 10 to 1 μm. At a cell voltage of 0.4 V, the current density was almost doubled. On the contrary, to get rid of the liquid water under high humidity conditions, MPL's porosity need to be increased and its thickness reduced [99]. The simulations presented in Ref. [99] showed that by increasing the MPL porosity from 0.2 to 0.5, the liquid water flux through the GDL can increase by around 9 times (e.g. at a porosity of 0.5, the flux was $4.505 \times 10^{-3}$ kg $s^{-1}$ $m^{-2}$).

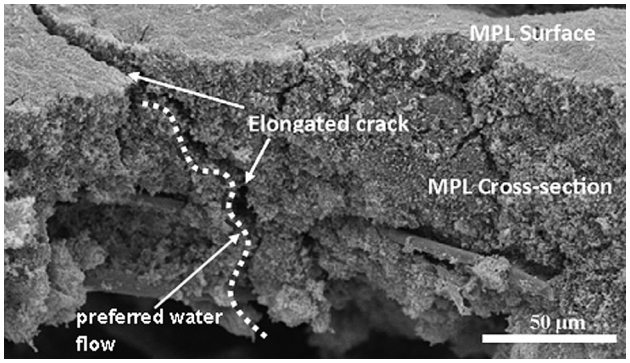


**Fig. 1.** (a) Cross-sectional SEM image of MPL of SGL 10BB type h (Reproduced from Ref. [97] with permission).

More advanced designs were developed such as graded-porosity type MPL (GMPL) where porosity decreases from the inner layer MPL/membrane to the outer layer MPL/GDL to facilitate the transport of liquid water through larger pores and gas diffusion via small pores [100]. Another design was a GDL modified hydrophobic/hydrophilic double micro porous layer (GDBL) that contains a hydrophobic MPL on the surface of the GDL and a hydrophilic MPL in the middle acting as an internal humidifier due to its water adsorption ability [101].

Despite all these modifications in the design of MEA, the effect of the cell operating conditions on water distribution and transport remains most pronounced. Operating PEMFC with high relative humidity gases increases the risk of flooding in the cell [102,103]. They showed that cathode channels become more flooded with liquid water as RH of reactant air increases from 26% to 66% for the same current density (e.g. 0.8 A $cm^{-2}$) [102]. When they operated the cell with dry air of 26% RH, liquid water was visible in the channels only when the stoichiometric air flow was set to 2.5 and below. Meanwhile with 66% RH of air, water was still present even at higher stoichiometric values.

Generally, flooding can be prevented by running the cell with high stoichiometric flow rates [104] or elevated temperatures [105–107]. Ous and Arcoumanis [106] found that flooding in the cathode channels can be overcome by raising the temperature from 30 °C to 60 °C under the testing conditions shown in Fig. 2. The benefit of using heat as a mechanism for water extraction from the cell can be extended to the polarisation performance of the cell. Increasing the operating temperature of the cell enhances the rates of electrochemical kinetics of the catalyst [108–110]. In Ref. [108] an explanation was given of how high temperatures affect the electrode reversible potential (thermodynamic open circuit voltage), Tafel slope, and exchange current density. At temperatures above 100 °C, the reduction in the electrode reversible potential is less due to the change in the reaction entropy (e.g. gaseous reactants are converted to gaseous product instead of liquid). To be noted is the improvement with temperature in the exchange current density and Tafel slope for both hydrogen oxidation reaction (HOR) and oxygen reduction reaction (ORR).

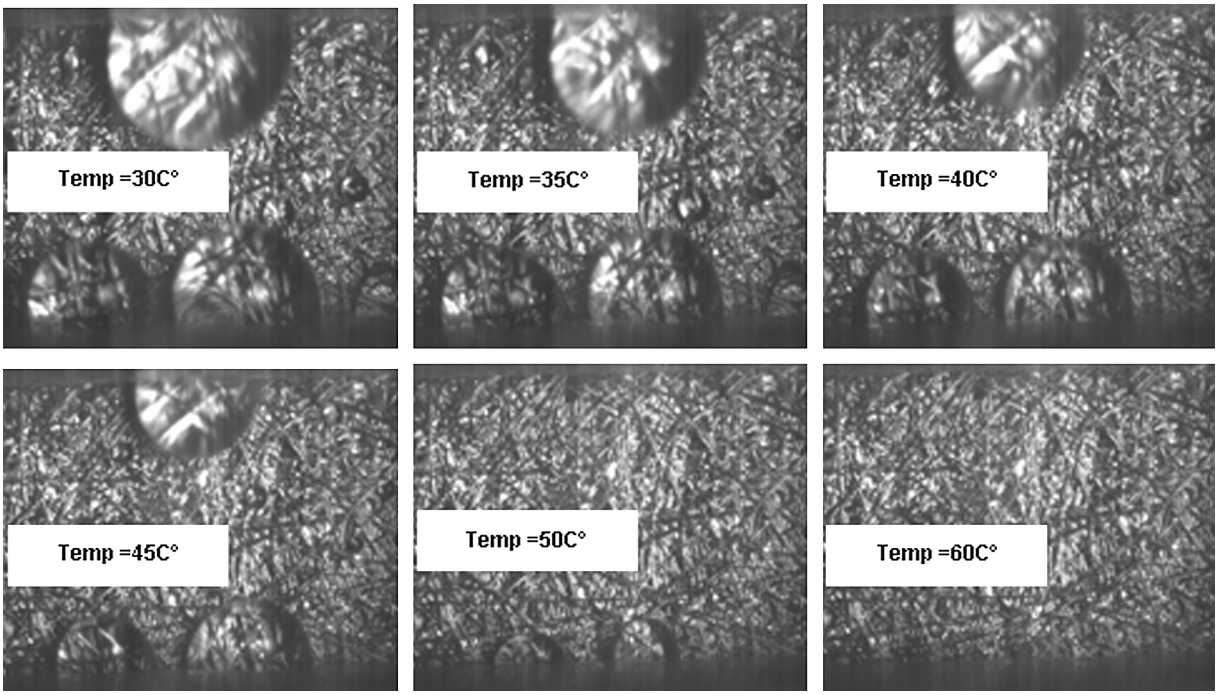


**Fig. 2.** Images of water accumulation in the cathode flow channels for different fuel cell operating temperatures [106].

Currently, major research activities are focussing on the development of next generation membranes that can operate efficiently at high operating temperatures (≥100 °C) [111–119]. If successful, issues related to water management, cooling, CO tolerance of the cell etc will be much simplified [108,120]. Further development of these high temperature membranes is required to extend their limited life-time and durability beyond 1000 h [121–123]. The phosphoric acid-doped polybenzimidazole electrolyte high-temperature membranes presented in Ref. [121] was able to operate only for 1220 h despite the low current density (0.2 A $cm^{-2}$). When they tested the cell under 190 °C, the cell voltage started to drop significantly after 1000 h of operation and by 1220 h the voltage was zero. The same type of membranes was examined in Refs. [122]; considerable hydrogen cross-over was reported after 510 h of continuous testing at 714 mA $cm^{-2}$ followed by 90 h of intermittent testing at 0.3 A $cm^{-2}$ which was due to the physical degradation of these membranes including agglomeration of the electro-catalysts and membrane thinning.

A number of visualisation techniques were applied to monitor the water distribution and transport in different parts of PEMFC including fluorescence microscopy [124], Environmental Scanning Electron Microscope (ESEM) [87,125], X-Ray radiography [126–132], X-Ray tomography [133], neutron radiography [134–136], magnetic resonance [137], and video cameras [138–142]. An overview of these experimental techniques can be found in Refs. [143,144]. Similarly, several two-dimensional and three-dimensional based models were developed to simulate the multi-phase flow of gas and/or liquid water in the membrane [145–147], GDL [148–153], CL/MPL/GDL structure [154,155], and cathode gas flow channels [156–159]. These studies have provided detailed understanding of in-plane and through-plane water accumulation and transport within these micro porous layers.

The water produced by the cell appears first at the catalyst layer of the cathode where oxygen reduction reaction (ORR) takes place. Depending on the hydration state of the membrane, water can either travel to the electrolyte to support the back diffusion stream or in the opposite direction towards MPL. Due to the hydrophobic nature of MPL, the formation of water films at the catalyst will be prevented and the access of product water to GDL will be limited [130]. The X-ray visualisation of [130] showed high-resolution cross-sectional images (with spatial resolution of 0.8 μm) of water in-situ distribution for two types of GDLs, with and without MPL. From these images, it can be seen that water saturation in the GDL without MPL (Fig. 3a) was significantly higher than the one with added MPL (Fig. 3b). In the later case, water droplets appeared on the surface of the GDL because of the highly hydrophobic MPL.

The water in the GDL is subject to viscous, capillary and gravitational forces. The fact that the capillary number (the ratio of viscous forces to interfacial tension forces) is relatively small, implies that water transport in GDL is dominated by capillary diffusion. The simulations of [153] using mean value model (MVM) confirmed that the capillary force is the main mechanism to drive the water flux within the GDL.

The distribution of the liquid water is strongly affected by the geometry of the GDL structure [149] and weakly by the cross leakage gas flow streams [135]. Water tends to accumulate initially more under ribs or lands than under channels [129,130,148,152] which is probably expected since air will have less access and longer diffusion length to reach those regions and remove liquid water. The images captured by Ref. [130] and presented in Fig. 4a and b show clearly higher concentration of liquid water under the rib area for the two types of GDLs, with and without MPL, at a current density of 0.4 A $cm^{-2}$. Water starts to build up close to the channel walls forming liquid films as a result of the hydrophilic capillary force of the walls and the drag force of the gas flow in the flow channels [142]. As water continues to penetrate the GDL, particularly at high current densities, the water accumulated under the channel regions travels first towards the air flow channels [155] developing on the surface as droplets [130,141]. Fig. 3a and b illustrates how by increasing the current density to 0.8 A $cm^{-2}$ the GDL without MPL (24BA type) becomes flooded with liquid water whereas the addition of MPL (24BC type) leads to droplets appearing on the surface of the cathode channels.

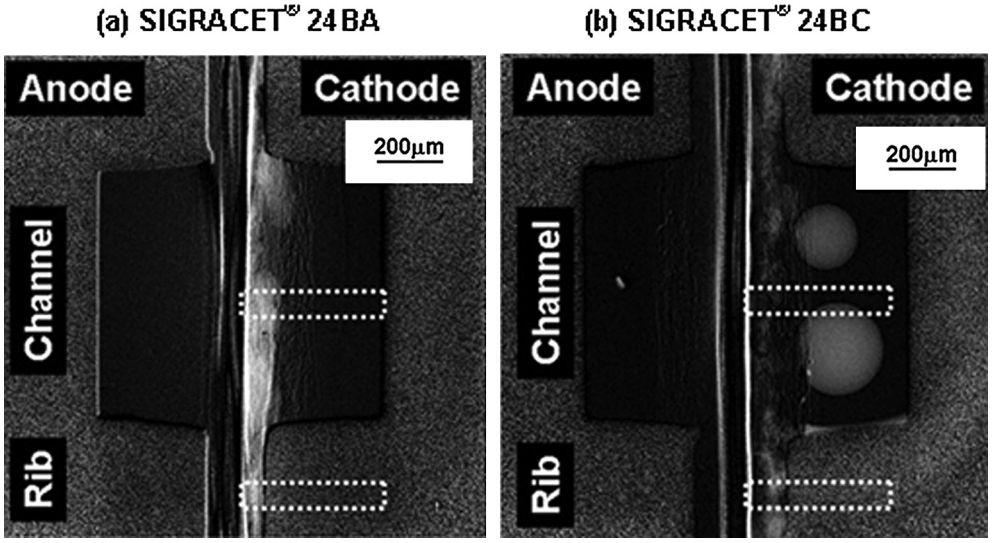


**Fig. 3.** Cross-sectional images of water accumulation under channel and rib area at current density of 0.8 A $cm^{-2}$ for (a) SIGRACET® 24BA; and (b) SIGRACET® 24BC h (Reproduced from Ref. [130] with permission).

The detachment of droplets from the surface of GDL occurs when droplets become larger in size as illustrated in Fig. 5 [139]. Ous and Arcoumanis [139] showed that droplets with size larger than 0.4 mm can detach from the surface of GDL (Toray TGP-H-060) by an air velocity below 60 m $s^{-1}$ whereas smaller droplets maintain their direct contact with the surface. The reason for this is that bigger droplets have larger contact surface area with the flowing air. When the aerodynamic force of the air flow gradually increases, droplets lean to the opposite direction of the air flow until they reach their critical contact angle and detach completely from the surface [139]. In Ref. [159] values for the critical receding contact angle are reported to be in the range of 50–80 °C for carbon papers and around 90 °C for carbon cloth.

The structural properties of GDL such as porosity and surface roughness [157,159,160] were found to have an effect on the contact angle and pinning phenomena. In Ref. [159] the static and dynamic contact angle of water droplets on different GDL designs including carbon cloth and carbon papers were measured and found to be different. For example, static angle of droplet with size of 1.2 mm on a carbon paper type 1 was ~120 °C. For a similar droplet size, the static angle on carbon paper type 2 and carbon cloth was 136 °C and 140 °C, respectively. Also the design aspects of flow channel plates including channel height [157], channel-land ratio [161] and flow patterns [162] play a significant role on droplet deformation and detachment. When the height of the channel increased from 250 to 500 μm in the simulations, a change in the evolution of water droplet shape in the flow channels was observed [157]. With higher channels, droplets tend to grow bigger in size keeping the flow field in the channel more uniform. Thus shearing stress and pressure difference on the interface of the water droplet become relatively weaker.

Based on these design considerations, it is clear that unless the stoichiometric air flow is high water slugs will develop leading to flooding in the cathode channels [106]. It was shown by Ous and Arcoumanis [106] (Fig. 6) that water disappeared completely from the channels only when air stoichiometry ($\lambda_{air}$) reached the value of 36. Below that stoichiometric point, water films start to evolve from the channel walls and gradually grow in size until they merge and block the access of the air flow in the channels.

Direct visualisation techniques can reveal the location of water flooding in the flow channels of an operating cell. If optical

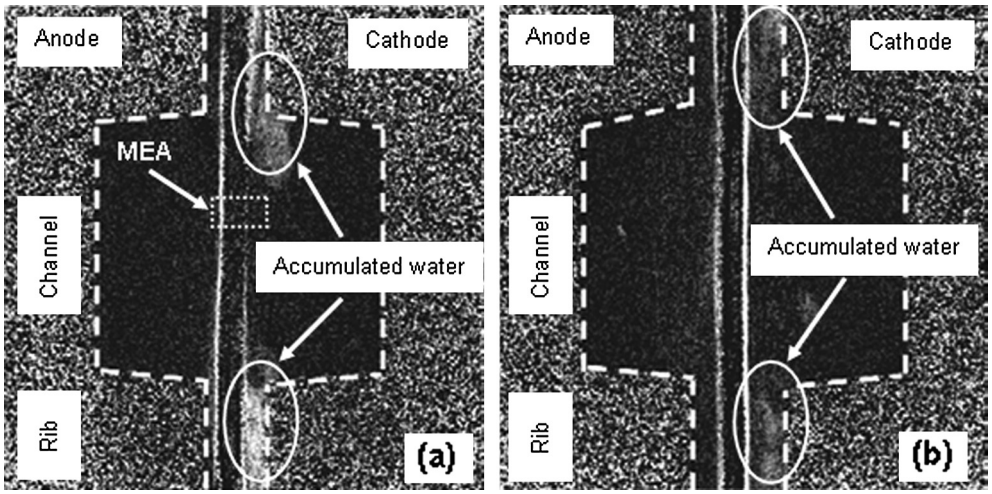


**Fig. 4.** Cross-sectional images of water accumulation under channel and rib area at current density of 0.4 A $cm^{-2}$ for (a) SIGRACET® 24BA; and (b) SIGRACET® 24BC h (Reproduced from Ref. [130] with permission).

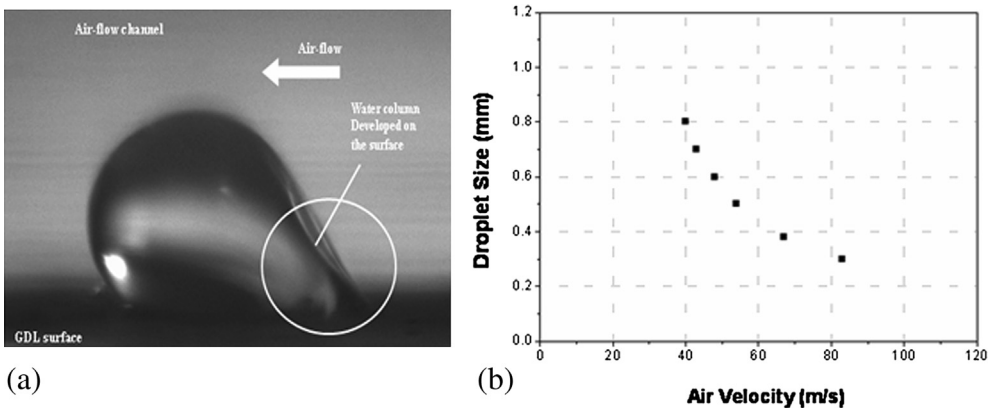


**Fig. 5.** (a) Image of droplet detachment from the GDL surface by the air flow (b) Air velocity detachment for different droplet sizes [139].

accessibility to the channels is not feasible, current density distribution or temperature distribution measurements of the cell, also called mapping, can assist in predicting the water concentration profiles across the membrane. The correlation between water, current and temperature was investigated in many studies [163–171]. In general, water tends to accumulate near the outlet of the cathode flow channels despite the appearance first of reactant air at the inlets. The fact that the air velocity reduces gradually along the

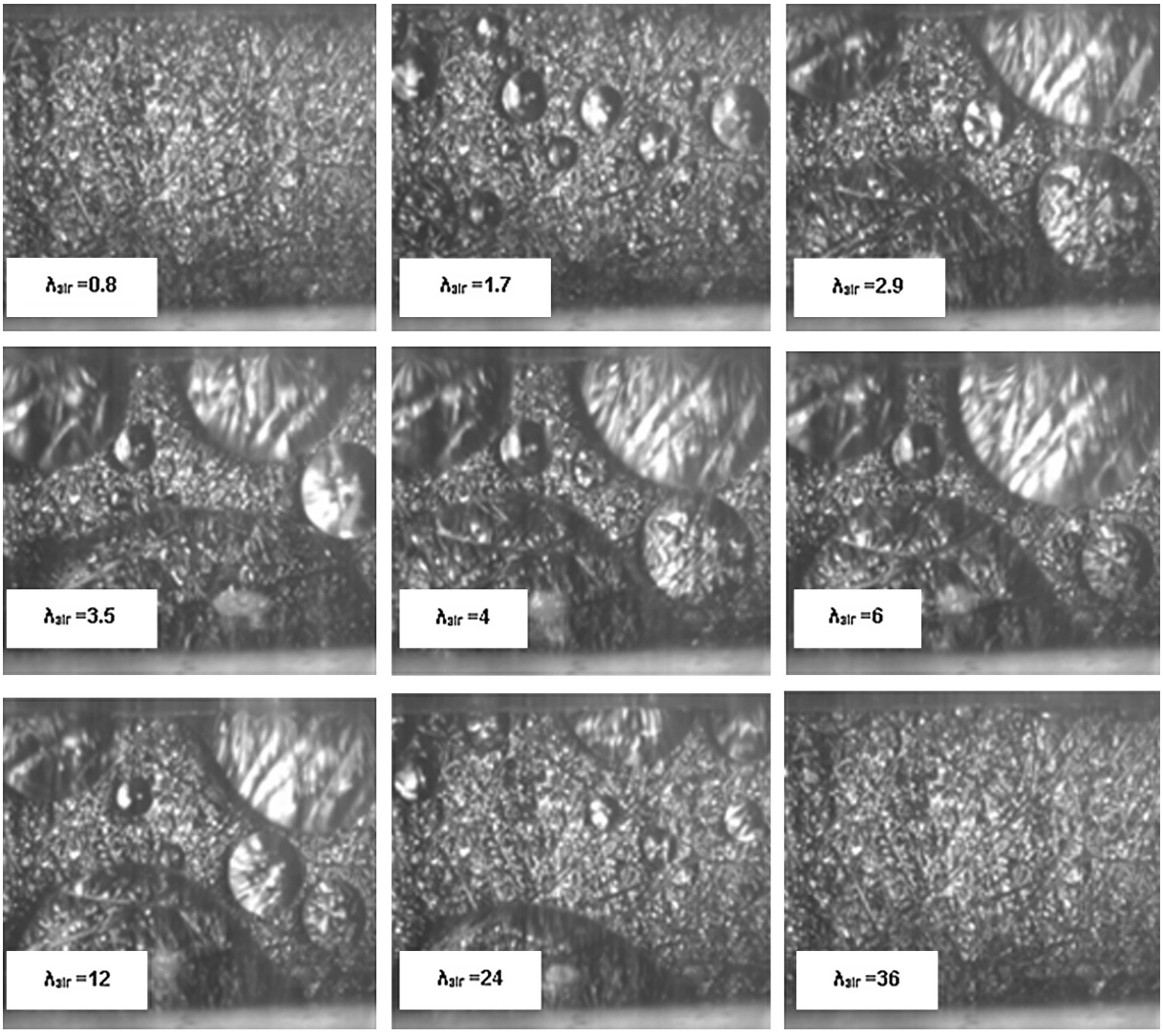


**Fig. 6.** Images of water accumulation in the cathode flow channels within a range of operating air stoichiometry [106].

flow channels enables more formation of water droplets on the GDL surface towards the channel exit. In Refs. [172,173] there is an agreement that water accumulation takes place at the exit of the flow channels based on their optical observations. The higher the air velocity at the inlet (e.g. 16 m $s^{-1}$ vs. 7.4 m $s^{-1}$ at the outlet [173]) the more sufficient it is to remove any liquid water from those regions. The calculations carried out by Ref. [174] have suggested different trends. The velocity of the air flow was lowest in the middle channels may be because of the effect of cell back-pressure that kept the air velocity high at the exit of the channels.

## 3. Water production

It is likely that the best way to assess the effect of water formation on the PEMFC durability is to understand the electrochemical reaction of the cell in more depth. The formation of by-product water takes place on the surface of Pt particles within the cathode catalyst layer by two gas-phase reaction pathways: $O_2$-dissociation and OOH-formation [175]. In the $O_2$-dissociation pathway, dioxygen adsorbs on the Pt surface [176] and dissociates. Each oxygen atom then reacts with chemisorbed hydrogen atoms to form water. Similar outcome exist from the OOH-formation pathway as a hydrogen atom on the surface first reacts with adsorbed $O_2$ to form OOH. This then dissociates to form chemisorbed OH and O which react with other chemisorbed hydrogen to form water. According to [175], the OOH-formation is more favourable for the cathode reaction due to its higher energy barrier of the dissociation step (i.e.17 kcal $mol^{-1}$). However, the fact that water is generated at the catalyst makes the catalyst structure more exposed to deterioration through the water formation process than other parts of the cell.

The design of the catalyst structure consists of three main components: an electronically conducting material (Pt/C), an ionically conducting material (perflurosulfonate ionomer (PFSI)), and an electronically and ionically insulating material (PTFE). These components are randomly distributed in the form of clusters bridging the Nafion membrane with current collection sites, as illustrated in Fig. 7. Gaseous reactants and liquid products are able to penetrate through the void regions of these clusters; the distribution of clusters and the ratio of particles loading (e.g. % Pt/C vs. PFSI vs. PTFE) determines the catalyst utilization [177].

### 3.1. Catalyst deterioration

#### 3.1.1. Pt and ionomer dissolution

In Pt/C clusters within the catalyst layer, Pt particles are deposited on a relatively larger carbon support as shown in Fig. 7. During the electrochemical reaction of the catalyst, these nanocomposites undergo structural changes in terms of Pt concentration and distribution. These changes, also known as the loss in the

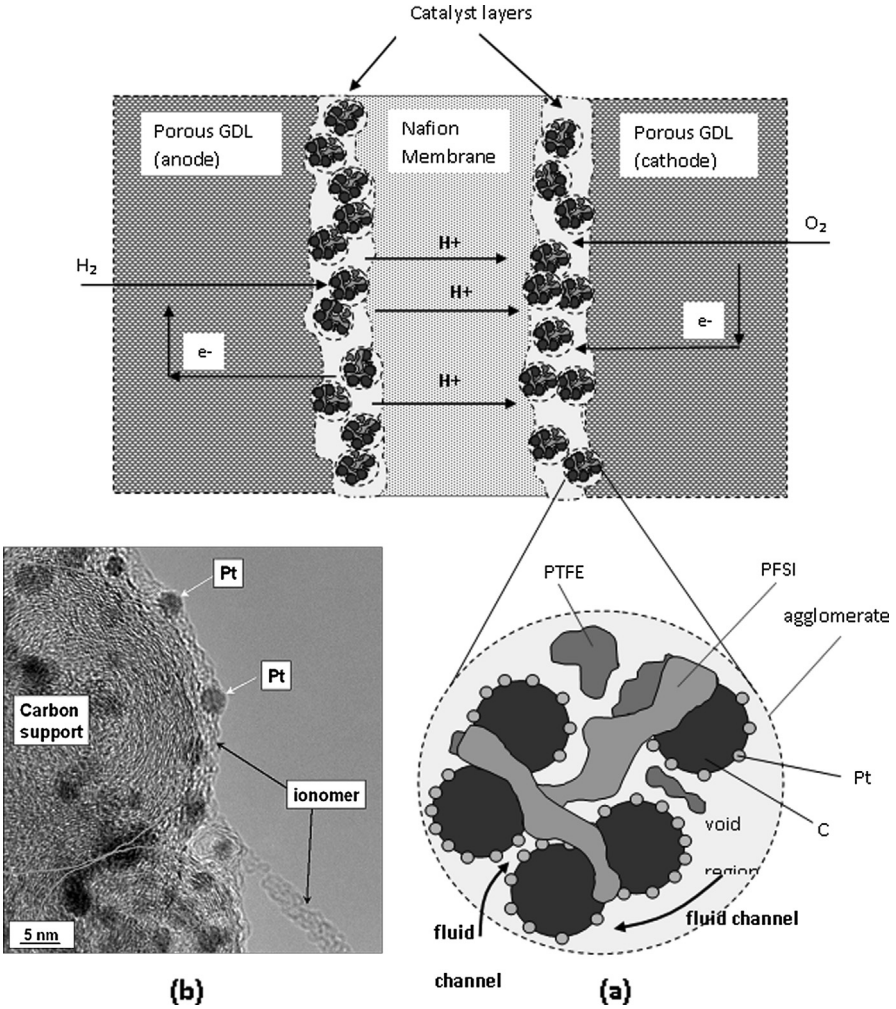


**Fig. 7.** (a) Cross-sectional view of a typical membrane electrode assembly (MEA) of PEMFC (b) TEM image of Pt catalyst particles on carbon support surrounded by recast ionomer h (4(b) is reproduced from Ref. [351] with permission).

active surface area of the catalyst, were associated in previous studies [178–180] with four main mechanisms: (a) Ostwald ripening (b) Pt crystal migration and coalescence (c) detachment and agglomeration of Pt nanoparticles, and (d) dissolution and reprecipitation of Pt single crystals in the ionomer and membrane.

Figs. 8 and 9 show TEM images presented in [352] of $Pt_3Cr$ and Pt particles agglomeration at the cathode and anode catalyst layers, respectively, after cell operation. At the catalyst cathode, Fig. 8, $Pt_3Cr$ particles were enlarged to almost twice their original size after 500 h of testing. The size has changed from ~3 to 10 nm in the fresh cathode layer to ~6–20 nm. Coarsening of Pt particles was more severe at the catalyst anode as shown in Fig. 9. After 1000 h of testing, Pt particles at the anode-membrane interface not only increased in size (e.g. from 1–12 nm to 20–40 nm) but also changed in shape to cuboidal with faceted sides.

Potential cycling is considered to be the main cause of coarsening and coalescence of Pt particles in the catalyst. The effect of cycling becomes more noticeable with an increased number of applied cycles [185–189] as well as with changing the profile and frequency of these cycles [181–184]. In Ref. [182] it has been reported a 75% loss of Pt surface area after varying the cell voltage between 0.65 and 1.05 V for 10,000 potential cycles. The Pt loss above 1 V of cell voltage was also found high in Ref. [181] and its cause associated with Pt grain growth. The voltage level in Ref. [184] was slightly lower (e.g. 0.95 V) but for more testing cycles (15,000 cycles). They also examined two cycling profiles (square and triangle) and found that the loss of Pt mass activity per hour is almost doubled when the cycle period is halved. The loss was higher for the square wave than the triangular cycle profiles (e.g. 4 vs. 1.8 $\mu A\ mg^{-1}\ cycle^{-1}$). The catalyst surface area was reduced dramatically by more than 50% from 70 to 30 $m^2\ g^{-1}$ after 15,000 testing cycles. This was in agreement with the results of [183] where it was found that when alternating voltage cycling (0.5–1.3 $V_{RHE}$) is applied with square waves of 30 s time period, the active surface area is reduced by 40% (50–30 $m^2\ g^{-1}$) just after 200 min of operation.

The results data obtained in Refs. [183,184] were at much higher level than the measurements of [185]. After 3000 of $H_2$/air cycles, Pt reduction from the cathode and anode by 15.6 and 6.3% of their initial ECAs of 55.4 and 54.2 $m^2\ g^{-1}$, respectively was observed [185]. Different results were obtained by other researchers: 70% reduction after 83,000 cycles (80–27 $m^2\ g^{-1}$) [188], 25% after 400 cycles [186], and ~50% after 2400 cycles [189]. Logically, the higher the number of test cycles, the higher the Pt loss from the surface area of the catalyst. However, direct comparison is difficult because of the many influencing factors that cannot be quantified accurately like the case of the technique used for Pt deposition on carbon support, the type of surfactant for Pt nano-particles [190] as well as other design and operational factors concerning the cell.

It is not clear yet whether water formation plays a role in the coarsening and coalescence of Pt particles. Only few reports have highlighted the effect of water on the growth of Pt particles [191,217], Pt adsorption [176], and Pt migration [192,352]. In Ref. [191] it was agreed that the hydration level of the catalyst influences the crystallite migration particle growth mechanism. The particle size of the cathode and anode electrodes was found, therefore, to be different. This was based on their Pt distribution curve measurements and on the expectation that the presence of liquid water lowers the activation energy for the particle's growth. The review of [217] pointed to the fact that by increasing RH the Pt-particle size would also increase. Again, it is not easy to identify the cause since the increase in Pt size could simply be due to water flooding at the catalyst layer rather than enhancement of ORR and thus water formation. Also the loss in the active surface area of the catalyst by Pt migration could also be caused by water transport in PEMFC since once Pt particles are detached from their carbon support, they become vulnerable to further displacement; this is discussed in more detail in Section 5.

As Pt particles dissipate from the catalyst layer during the cell reaction, so does the catalyst ionomer [36]. Previous studies associated the dissolution of ionomer from MEAs to a number of factors such as hydrogen crossover [198], Nafion loading [197], and cell operation under OCV [44,199] and extreme relative humidity conditions [30,200]. However, none of these studies associated the segregation of ionomer to the water production process in PEMFCs. Probably the best way to detect this is to monitor the change in the concentration level of fluoride ($F^-$) and sulphate ($SO_4^{2-}$) anions of the cell. According to a number of studies, the change in $F^-$ and $SO_4^{2-}$ concentration is attributed to the variation of the relative humidity of the reactant gases. The effect of the relative humidity on the fluoride emission rate from the cell is discussed in Section 5.1.

### 3.1.2. Carbon corrosion

Carbon corrosion was detected in many occasions following the operation of the cell under potential cycling [181,183,187,193], start-

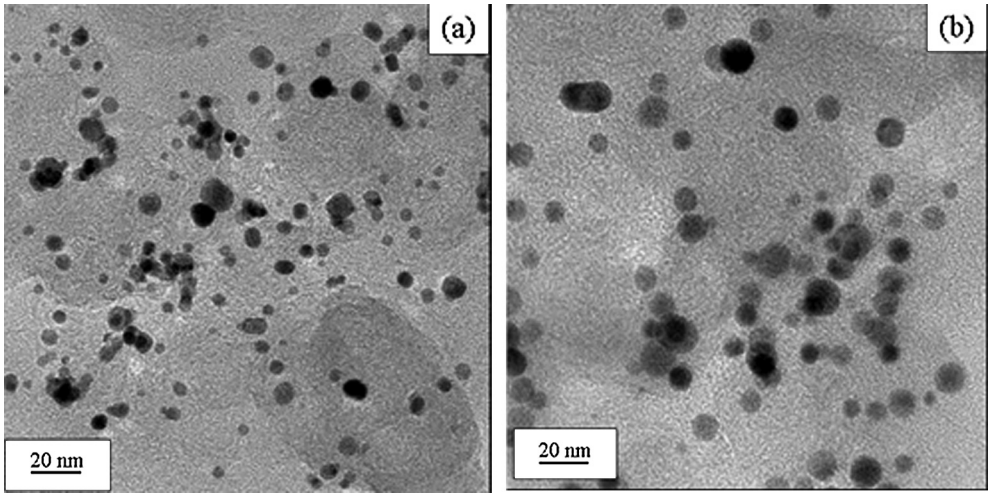


**Fig. 8.** TEM images of $Pt_3Cr$ catalyst particles in (a) fresh cathode catalyst layer and (b) cathode catalyst layer in MEA electrochemically aged for 500 h (Reproduced from Ref. [352] with permission).

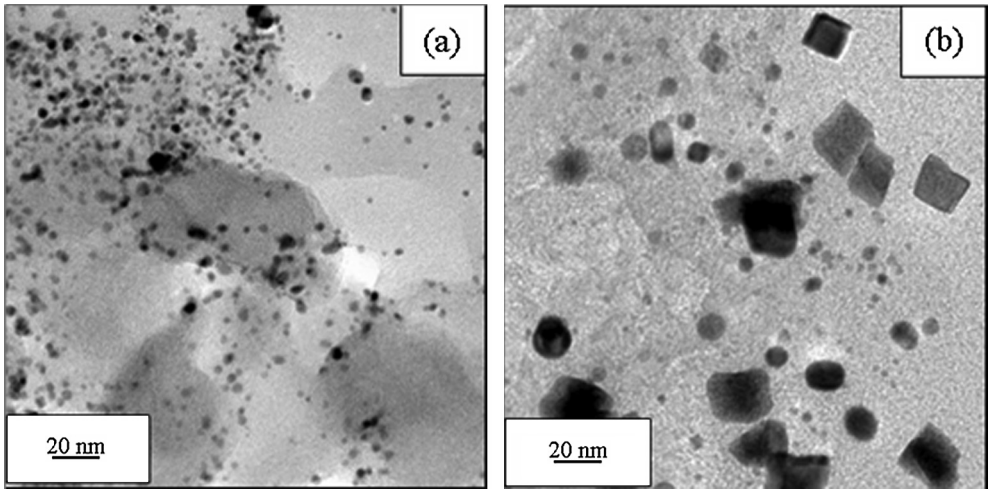


**Fig. 9.** TEM images of Pt catalyst particles in (a) fresh anode Pt catalyst layer and (b) Anode catalyst layer at anode–membrane interface in MEA electrochemically aged for 1000 h (Reproduced from Ref. [352] with permission).

up and shutdown [175], localised fuel starvation [194,195], and extended OCV [196]. Wilson et al. [191] presented TEM images showing how potential cycling causes considerable dissipation of Pt particles from their carbon support in the catalyst. After 2 and 4 h of cycling between 0.4 and 1.4 V, the amount of Pt decreased to about 71% and 47%, respectively.

The stability of Pt particles is strongly affected by the corrosion of their carbon support during the electrochemical reaction of the cell. Ball et al. [187] attributed the poor stability of Pt particles in their tested catalyst to the dissolution/sintering of carbon. They calculated the cumulative carbon corrosion for a range of commercially available and heat treated carbon blacks, e.g. expressed as maximum weight loss in wt%, and found that high area carbons are 25 times more corrosive than low area or heat-treated carbons. The increase in specific surface area of the carbon substrate in Pt/C catalyst tends to influence the carbon corrosion process. When Okada et al. [301] examined different surface areas of carbon substrates the ones with the largest area caused more Pt dissolution from the catalyst and higher $CO_2$ generation rate from the cell. This result is probably expected since larger carbon particles will normally support more Pt particles on their surface and hence the damage would be more pronounced.

### 3.2. Mitigation strategies

New alloys were developed to enhance the performance and durability of Pt-based catalysts. The aim was to (1) improve the catalytic ORR activity (2) minimise the loss of Pt particles from the active surface area of the catalyst, and (3) make carbon-support more resistant to corrosion. One way to achieve this is to reinforce the design of the catalyst by impregnating Pt particles with substances that increase their stability on the carbon support. Platinum–Titanium (Pt–Ti) and Platinum–Ruthenium/Carbon (Pt–Ru), for example, were suggested by Ref. [201] as suitable alloys with high Pt stability under severe acidic conditions. When these alloys were utilised in the design of MEA, the cell was more CO-tolerant than pure Pt catalyst as deduced from the negative shift measurements of the cell potential. Their results also showed that these alloys have better ORR activity than pure Pt catalysts, hence higher kinetic current densities of the cell.

Cobalt (Co) is another metal that can potentially improve the stability of the catalysts. The fact that their bond dissociation energy with Pt particles is relatively high ($\sim$1072 kJ mol$^{-1}$), makes them suitable candidates for Pt-based catalysts; Pt–Co based alloys have been tested in previous experimental investigations [187,188,202–204] and showed improved cell polarisation performance compared to conventional Pt/C catalysts. Based on Ref. [188], the mass and specific activity of the Pt–Co cathode catalyst is 2$\times$ and 4$\times$ higher than Pt/C catalyst, respectively. The loss in the surface area of Pt–Co catalysts tends to be quite slow reaching a maximum of 43% after 83,000 potential cycles (35–20 m$^2$ g$^{-1}$). However, the measurements of Ball et al. [187] did not show any sign of loss in the surface area of Pt–Co catalysts after cycling. This was the case except for when the catalyst was immersed in 1 M $H_2SO_4$ solution.

The effect of Co on Pt stability of the catalyst was demonstrated in Ref. [202] by capturing transmission electron microscopy (TEM) images of the catalyst structure in the presence and absence of Co after 10,000 operating cycles. In Pt/C-based catalysts, Pt particles migrate towards the membrane layer whereas this was not the case with the PtCo/C design. To enhance the stability of Pt–Co even further, Tada et al. [203] suggested replacing the conventional carbon black with new carbon support that has optimal combination of carbon surface area and PtCo particle size ($\sim$800 m$^2$ g$^{-1}$, PtCo $\sim$4–5 nm). This proposed design exhibited high ORR activity of the catalyst as evident from the polarisation results of the cell.

An alternative method to minimise the loss of Pt from the active surface area is to change the actual design of the catalyst. Instead of bonding Pt particles chemically to the surface of the carbon support, Pt atoms can be encapsulated inside a fullerene cage. This new type of catalyst, known as metallofullerenes, is considered to be one of the most promising designs to extend the lifetime of PEMFC [205]. Fullerenes can be in different shapes, such as spherical (buckyballs), cylindrical (carbon nanotubes or buckytubes), or an aggregate of cylindrical in the form of thin sheet (buckypapers). Relevant research focuses mainly on buckypapers amongst other types of metallofullerenes based catalysts. The design of these newly developed catalysts consists of single-walled nanotubes (SWNT), double-walled nanotubes (DWNT), multi-walled nanotubes (MWNT), or carbon nanofibers (CNF). Various techniques were used for the preparation of these catalysts such as ion exchange [206], borohydride [206], ethylene glycol reduction [207], direct sputter deposition [208], and electro-deposition method [209].

Wang et al. [206] examined the ion exchange preparation method against the borohydride method on MWNT for the same Pt loading. They found the ion exchange technique to be more effective in terms of ORR and Pt utilization; the later can be further improved by using nanotube-based catalysts. This claim was supported by the measurements of [208–211] which showed high polarization performance of the cell. The good accessibility to reactant gases and the uniform distribution of Pt on the carbon structure are not the only advantages of these catalysts, but good durability as well. Chen et al. [207] measured the degradation rate of MWNT, DWNT, and SWNT-based catalysts against commercial Pt/carbon black under an accelerated durability test (ADT). The ratio of Pt loss from the active surface area was reduced after 1000 cycles by around 1.5 times when using Pt/MWNT or Pt/DWNT and by 1.2 times for SWNT compared to a typical Pt/C catalyst. All of these catalyst designs had the same initial Pt concentration, which was in the range between 63 and 65 $m^2\ g^{-1}$, for accurate comparison. The loss in Pt/C was 48%, while in Pt/MWNT/Pt/DWNT and Pt/SWNT it was 32% and 38%, respectively. This reported value of Pt loss in SWNT (e.g. 1.2 times) was much lower than that detected in Ref. [210] (e.g. 3.8 times). After 400 h of ADT, the loss of Pt from the active surface area using buckypaper support was 18% while the Pt loss was 69% in Pt/C. The difference between these two results could be attributed to the design aspects of the tested cells as well as to some of the operating conditions such as the level of voltage cycling [210].

The use of different substances other than carbon for Pt-based catalysts was previously investigated with materials like aluminium oxide ($Al_2O_3$) [212], titanium dioxide ($TiO_2$) [213], zirconium dioxide (S–$ZrO_2$) [214], and tin dioxide ($SnO_2$) [215]. The advantage of using $Al_2O_3$ or alumina as catalyst support is due to its insulating characteristic. Since electron transport through the carbon support contributes to the growth of Pt particles, insulating-type support could prevent the passage of electrical paths, thus suppressing degradation.

On the other hand, when Pt-alumina catalyst was examined [212], Pt particles have remained almost the same size (~8 nm) after immersing it in deionised water at 80 °C for one week. Suzuki et al. [214] used different catalyst design, e.g. Pt–S–$ZrO_2$, and kept its electronic conductivity to a level where the ohmic loss of the cell is minimal. The performance of this catalyst was better than Pt/C when Nafion ionomer was not added to the design. The open circuit voltage of the cell (OCV) using a Pt–S–$ZrO_2$ cathode was slightly higher than the Pt/C type (0.883 vs. 0.868 V) and, at a current density of 2 A $cm^{-2}$, the cell voltage was 0.36 V compared to 0.31 V for Pt/C. Probably the best result was achieved in Ref. [213] when Pt/TONT catalyst was used. The active surface area of the catalyst was reduced by only 20.3% after 10,000 of accelerated potential cycles. This relatively small loss of Pt was purely due to the strong and stabilised physical interaction between Pt–Pt particles and Pt–TONT in the catalyst. Again this synergistic effect between Pt and TONT was the main reason for the improved ORR activities of the catalyst. The mass and area-normalised kinetic current densities at 0.8 V using a Pt/TONT catalyst was ~5.3× and 2.2× greater than the Pt catalyst, respectively.

Chen et al. [216] even suggested removing the carbon support of Pt particles completely from the design of the catalyst and use Pt/alloy nanotubes (PtNTs) instead. The idea was to alleviate most of the degradation pathways initiated by the carbon. This design was examined against Pt/C and Pt/carbon black catalysts and exhibited minimal reduction of the electrochemical active surface area. The Pt loss of PtNT, Pt/carbon black, and Pt/C catalysts was found 20%, 50%, and 90%, respectively after 1000 operating cycles. These values are significantly higher than those previously reported in Refs. [207,210].

## 4. Water retention and accumulation

### 4.1. Water retention

The presence of liquid water in PEMFC has a detrimental effect on the mechanical, electrical and chemical properties of the cell components. The deterioration of these properties can be attributed to three main mechanisms known as membrane swelling, corrosion, and ice formation.

#### 4.1.1. Membrane swelling

Swelling occurs as a result of water absorption by the membrane which expands its polymeric matrix. When liquid water is absorbed, the ionic constituents within the membrane become surrounded by those water molecules while the polymeric matrix resists the uptake of more water. The water inside the membrane increases its pressure relative to the external water surrounding the membrane due to the effect of the elastic forces of the polymeric matrix. The pressure difference between the internal and external water, known as swelling pressure, determines the increase in the partial molar volume of the solvent as a function of the operating temperature, water activity, compression load, and relative humidity [219–221,225,226]. The neutron-based images presented in Ref. [220] showed the changes in the physical dimensions of the PFSA type membranes under wet conditions; e.g. the thickness of these membranes was increased by 0.1 mm. Parrondo et al. [219] explained that such change in the membrane matrix structure is strongly dependant on the water activities of the ionic solution. For example, when they treated the membrane with KCl solution, the membrane thickness remained the same whereas with HC1 and NaC1 solutions the thickness changed by 10% and 5.5%, respectively.

In general, swelling develops in an anisotropic fashion since membranes creep more in one direction than in others. Membranes have a different creep response depending upon their water content and the surrounding temperature. Majsztrik et al. [223] elucidate the effect of both temperature and water on the mechanical properties of Nafion by arguing that hydrophilic domains within the Nafion structure become stable when water interacts with the sulfonic acid groups whereas these domains break apart with increasing temperature. This combined and complex effect causes major changes in the number, strength and flexibility of the cross-links between the hydrophilic domains. In order to investigate this phenomenon, Majsztrik et al. monitored the viscoelastic response of Nafion under a range of temperature and hydration conditions. They found that the tensile creep strain of Nafion increases with increasing water activity, e.g. increase in RH, for the whole temperature range tested (25–60 °C). The measurements also showed that strain values become higher under wetter conditions at lower temperatures (25–50 °C) but reduce at higher temperatures (60 °C).

The increase in the membrane thickness, known as the membrane thickening phenomenon, introduces non-uniform local stresses that can contribute to the mechanical failure of membrane particularly in areas that are more exposed to compression by the assembly of the cell. The simulations carried out by Kusoglu et al. [224] showed how hygro-thermal loading affects the stress distribution profile in the membrane. The in-plane stresses were mostly driven by the swelling strain, particularly on both ends of the membrane where stress is higher due to cell clamping.

The change in the mechanical characteristics of the membranes is correlated to the level and number of RH operating cycles applied to PEMFC. This was examined in the experimental work of [233] where an increase of both parameters resulted in a significant reduction of the MEA ductility. The average strain-to-failure was reduced by around 40% (from 1.32 to 0.58) after 100 cycles in the

30–80% RH range. Also, the elastic modulus of the membrane was reduced from ~480 to 280 MPa when RH increased from 25 to 75%. These results which were validated using a finite element model, revealed the formation and growth of mechanical defects such as crack and crazing in the membrane and MEAs. Kusoglu et al. [236] were also able to simulate the trend of the in-plane stresses across the membrane during five humidity loading cycles (95–30% RH). It was clear from their results that the value of in-plane stresses differ depending on the local contact area of the membrane (e.g. either facing the flow channel or in direct contact with the channel land). Calculations made by Kusoglu et al. [235] revealed that residual stresses can be up to 10 MPa which may lead to delamination of the membrane and the gas diffusion layer and similarly the high in-plane stresses were associated to crazing and its growth. The simulations of [286] suggest that in-plane stresses are much higher under the land regions than under the flow channels at any level of relative humidity of the reactant gases. For instance, at 0.05 swelling strain of the MEA under 100% RH, the in-plane stresses under the middle area of the flow channels were nullified.

The damage escalates further with additional tensile stresses when the membranes enter the dehydration phase in low relative humidity cycles. This can result in membrane thinning [229,230], delamination [231], or pinhole formation under extensive RH cycling [32,228,232]. Chen and Fuller [231] presented SEM images showing pinhole formation and signs of delamination on the surface of the membrane when operating the cell under low RH operation of 36%. The observed degradation was validated using a numerical model based on the main chain unzipping process of membranes. The simulations revealed that low humidity conditions enhance the side chain scission process creating many weak end-groups in the membrane's chemical structure, thus accelerating the degradation process. Similarly, the SEM observations of [230] revealed images of membrane thinning under relatively low humidity conditions of 65.8% at both the anode and cathode. As a result, the hydrogen crossover rate has increased gradually reducing the amount of hydrogen reactant; the degradation rate of the cell voltage was calculated to be around 0.0537 mV $h^{-1}$.

#### 4.1.2. Corrosion

The formation of hydrogen peroxide ($H_2O_2$) often occurs during the electrochemical reaction of PEMFC. This introduces dangerous radicals such as hydroxyl (OH) and hydroperoxyl (OOH) radicals that can potentially attack the membrane and accelerate the chemical degradation process of the cell. Based on [239], these radicals tend to alleviate the interface between the catalyst and ionomer and as a result, the active surface area of the catalyst is significantly reduced. The relative humidity of the reactant gases was linked in some way to the formation rate of $H_2O_2$ [238]. Sethuraman et al. [237] found noticeable differences in the amount of $H_2O_2$ generated at the cathode between dry and full humidity conditions. At a testing temperature of 95 °C, the rate was reduced 7× as RH increases from 0 to 100% (0.7–0.1 mol $cm^{-2}$ $s^{-1}$ × $10^6$).

Despite the majority of studies blaming voltage cycling of the cell for the carbon corrosion in PEMFC [183,184,186–188,217,240], some studies have associated its cause to the presence of liquid water in the catalyst [243–247]. Maass et al. [244] found that the corrosion rate of carbon is linearly dependant on the molar water concentration. For each $H_2O$ molecule present one molecule of $CO_2$ is formed. When they raised the molar water concentration by a factor of three (0.1–0.3) under anodic potential limit testing, the corrosion rate of carbon increased by an equal proportion (e.g. from ~2.4 to 7.2 g $h^{-1}$ $cm^{-2}$). This finding implies that the corrosion rate would be highest at the maximum current density.

The increase in the relative humidity of the reactant gases increases the risk of carbon corrosion at the catalyst. The measurements carried out by Stevens et al. [69] showed significant increase in the carbon combustion rate for XC72 and BP2000 type carbon support when the cell operation changed from dry to wet conditions. The carbon corrosion of the cathode catalyst layer in Ref. [332] was enhanced noticeably when the cathode inlet RH increased from 0 to 100%. The gradual decrease in the catalyst thickness (~70% reduction, e.g. 10.5–6.6 μm) and the increase in the carbon dioxide production at the catalyst (350–1,300 k ppm $s^{-1}$) confirmed the corrosion of carbon. Interestingly, RH was found to have negligible effect on the degradation rate of the anode catalyst as revealed from their back scattered Electron Microscopy (BSEM) images.

Corrosion can also affect the bipolar plates of the cell if no surface treatment is made to metallic-type plates to withstand harsh acidic and humid conditions [61,248,249,253]. Passive films can be formed at the interfacial regions between the cell components raising the overall ohmic resistance of the cell. This happens mainly at the interface with the gas diffusion layer creating additional interfacial contact resistance (ICR) with the bipolar plates; the thickness of this passive film determines the value of ICR. Antunes et al. [248] evaluated a range of materials from previous experimental investigations to find the best material for bipolar plates with minimum corrosion resistance.

Typically, the value of ICR reaches a maximum when the film reaches maximum thickness or stabilises in thickness. This was observed in Ref. [251] when ICR continued to increase from 200 to 320 mΩ $cm^2$ until the passive film reached maturity thickness after 30 min of cell operation. Stability of the passive film thickness was also detected in Ref. [252] where it took 50 min for the film to develop to a maximum thickness of 3 nm at 0.6 V in a simulated cathode environment against 20 min for 2.6 nm film at −0.1 V in an anode environment. It is worth noting that the thickness of passive films and the corresponding contact resistance will vary based on the compaction force applied to the cell assembly; the contact resistance gradient tends to be much smaller at large compaction forces.

Another effect of the corrosion of metallic bipolar plates is the release of metallic-based cations like $Fe^{3+}$, $Ni^{2+}$, $Cu^{2+}$, $Cr^{3+}$. The origin of these cations could be the dissolution of the alloys used as coating material for the plates. Using mass spectroscopy techniques, traces of chromium, nickel, iron, sulphur and aluminium from the by-product water were detected after operating the cell with aluminium plates coated with carbide-based alloy [42]. Their energy dispersive X-ray (EDX) analysis revealed more changes in Ni at the cathode than the anode which was attributed to the higher relative humidity as well as the electrochemical activity of the cathode. A list of major contaminants and their origins affecting the performance of PEMFC was identified by Cheng et al. [308]. Independent of the source of these impurity cations, they can potentially attack the membrane and deteriorate the mechanical and chemical stability of Nafion. Tawfik et al. [61] highlighted a number of cooling materials and techniques so that deterioration mechanisms like catalyst poisoning, reduction of membrane conductivity, passive film formation, reactant crossover, and bin-hole formation on bipolar plates can be prevented.

The change of the ionic conductivity of polymer membranes could be strongly affected by the amount of impurities in the cell [254]. Indeed, this was addressed in Ref. [255] when immersed membrane samples in sulphate salt solutions were used to understand the effect of inorganic cations. They found that the reduction in the membrane's conductivity is negligible at low impurity levels (e.g. 0.1, 1, 10 ppm) but becomes significant at high levels (100 ppm). They also demonstrated that the effect of each type of impurity can be different. For example, $Ni^{2+}$, $Cu^{2+}$ contaminated membranes displayed lower conductivity than

$Na^{+}$ ones whereas $Fe^{3+}$ exhibited the lowest conductivity amongst all.

*4.1.3. Ice formation*

The damage originated from the lingering water in the cell becomes more severe when liquid water turns into ice under subfreezing temperatures which can block the access of gases into the reaction sites of the catalyst causing gradual drop in cell's performance [257,258]. This was confirmed by the experimental measurements of [262] where the current density of the cell was reduced linearly as water continued to freeze. The phase transformation, caused by freeze–thaw cycles, also results in volume expansion of the retained water. This introduces local isotropic stresses that can damage the structure of the membrane and other porous layers of the cell including the catalyst, GDL, and MPL. The SEM images presented in Ref. [260] and reproduced in Fig. 10 show detrimental changes to the catalyst surface of a fully hydrated MEA under 10 freeze–thaw cycles at temperatures reaching −30 °C. Furthermore to the structural damage, the electrochemical active surface area of both the anode and cathode catalysts was reduced considerably, e.g. the cathode by 23% and the anode by 15% after 20 freeze–thaw cycles.

An early impact of ice formation on the MEA structure could be on affecting its porosity. The environmental scanning electron microscopy (ESEM) observations made by Alink et al. [267] revealed a significant increase in the porosity of a damaged MEA when wet stack underwent freeze/thaw cycling Fig. 11. This led to the exposure of the catalyst layer and further decrease in its surface area by Pt particles detachment. As it can be seen from Fig. 7, the damage in the cathode was more substantial than the anode probably due to its higher water concentration. Li et al. [261] revealed, based on their cryogenic FESEM analysis, that the porosity change across the catalyst layer due to ice formation is uneven. Eventually, the biggest change was at the interface region with the membrane layer (∼25%). This finding is not in agreement with the CRYO SEM observations of [262]. Although, both studies identified two distinct ice density regions in the catalyst layer, Kusoglu et al. [286] believe that the majority of ice is formed closer to the GDL side rather than the membrane. They based their theory on the fact that existing ice prior to subzero operation will melt by the reaction heat of the catalysts. Liquid water will therefore migrate away from the hot membrane to the cooler GDL and continue to freeze.

In addition to the change in porosity, ice formation can damage the structure of other parts of the cell [258]. This occurs more noticeably in regions of high water concentration within the cell. The damage detected by Lee et al. [38] under freeze/thaw cycles was more severe when MPL was added to the design of the cell. At a high current density of 1 A $cm^{-2}$, the degradation gradient in the cell voltage for the same number of test cycles was 4.3 with MPL against 3.2 without MPL. This is likely because MPLs capture most of the liquid water for sustaining the membrane and catalyst layers at desirable hydration state. The damage might equally be the same when the cell generates more by-product water at high current densities. The results of [38] showed that despite the above role of MPL, the formation of ice-sheet between the catalyst layer and GDL can be prevented which hastens the degradation of mass transport as well as increases the total polarization resistance of the cell significantly.

Morphological damages of the PEMFC components due to ice formation can have serious consequences on the performance and durability of the cell. This includes scenarios like fuel crossover [264,265], catalytic combustion as a result of pinhole formation [263,264], fuel/oxidant starvation caused by water flooding in cracked regions [131,266], accelerated catalyst erosion due to further exposure of the electrochemical surface area [26,267], and increase in the ohmic resistance of the cell reflecting the increase in bulk resistivity (interfacial contact resistance) of the damaged layers [75,268,269]. Visual evidence of pinhole formation and micro-cracking on the surface of the membrane is provided in Fig. 12a [264] following operation at sub-zero temperatures (e.g. cathode temperature below −5 °C). The cell voltage has decreased and suddenly collapsed to zero after four cycles even at the low current density of 350 mA $cm^{-2}$.

Ice formation can also lead to the delamination of catalyst layers. Water tends to accumulate and freeze forming ice lenses at interfacial regions adjacent to the catalyst layer, e.g. either between catalyst and diffusion layer or catalyst and polymer membrane. This phenomenon was highlighted in the simulations of [272] where formation of ice lens in the interfacial regions was predicted. Other experimental studies used in-situ optical techniques have also observed this phenomenon [264,271]. Fig. 8b shows an image captured in Ref. [264] of catalyst layer delamination from both the membrane and the gas diffusion layer (GDL) sides. According to their measurements, this delamination resulted in hydrogen crossover and consequent drop in cell performance. Similarly, in Ref. [44] the danger of delamination in oxygen crossover was pointed out which enhances the formation of hydrogen peroxide causing catalytic combustion at the anode.

The effect of catalyst delamination tends to be significant on the ohmic loss of the cell. Kim et al. [270] compared the change in cell

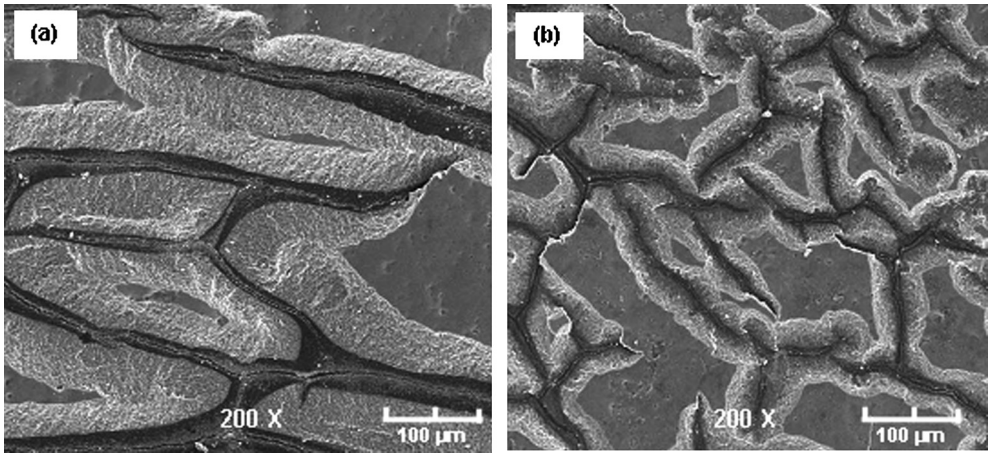


**Fig. 10.** SEM images of MEA without purging after 10 freeze–thaw cycles between 20 and −30 °C (a) anode (b) cathode (Reproduced from Ref. [260] with permission).

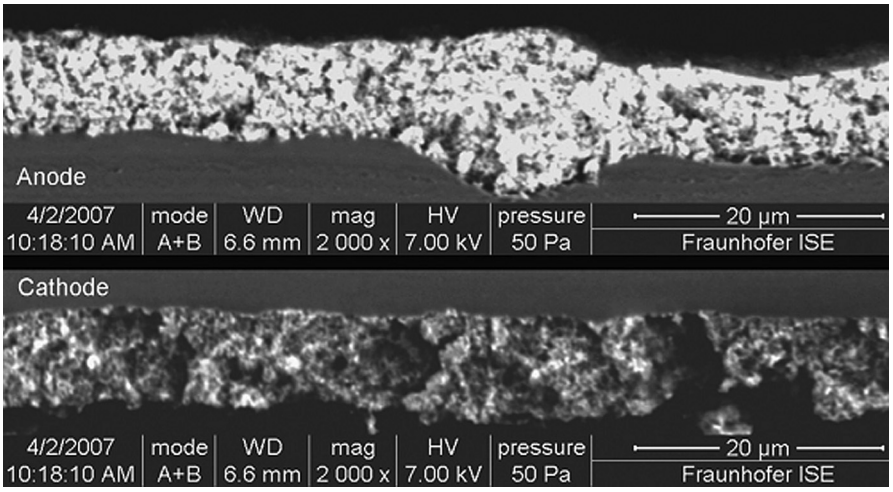


**Fig. 11.** Cross-section of MEA catalyst layers after 71 of freeze/thaw wet cycles (Reproduced from Ref. [267] with permission).

resistance caused by the delamination at membrane/catalyst (M/CL), catalyst/gas diffusion layer (CL/GDL), and gas diffusion layer/bipolar plate (GDL/BPP) interfaces. The increase in the interfacial resistance of M/CL and CL/GDL was much higher than that of the GDL/BPP. Their measurements showed that with a delamination area of 50 μm, the cell resistance was increased by around 30% for M/CL and CL/GDL but only 10% for GDL/BPP.

Delamination of the catalyst layer can also lead to higher loss of Pt particles from the active surface area of the catalyst. Yang et al. [271] were able to capture TEM images showing a gap at the interface between the cathode catalyst layer and the membrane. Consequently, Pt particles were increased in size (3 to 5–8 nm) followed by significant reduction in the specific surface area of the catalyst (~50%). Meanwhile, Ge and Wang [274] justified the 35% reduction in Pt surface area of their tested cell at −30 °C through the formation of an ice sheet between Pt particles and ionomers in the cathode catalyst layer.

Not all the residual water in the membrane freezes when the temperature reaches 0 °C. Three types of water molecules known as non-freezing water, bond freezing water, and free water were distinguished by researchers during subfreezing temperatures [275]. Each of these types has different freezing points depending on the nature of their molecular chemical bonds. For instant, Lu et al. [276] detected three distinctive water states in subfreezing temperatures using a dielectric relaxation spectroscopy technique. They found in the kHz frequency region that water molecules are hydrogen-bonded to the sulfonates whereas in the GHz domain water molecules are either in liquid bulk-like or loose bond forms.

As temperature drops to 0 °C, only the unbounded free water (bulk water) molecules transform into ice. The images presented in Ref. [277] showed that even at temperatures of −3 °C, liquid water is still present in the form of droplets on the surface of the catalyst. However, these droplets were not observed when the cold start was at −5 °C. This suggests that the freezing-point depression of water in the catalyst is no more than 2 °C. The generation of liquid water below 0 °C was again witnessed in Refs. [279,280] but the temperature of water freezing was even lower (e.g. −10 °C in Ref. [288]). Ishikawa et al. [279] attributed the reason for this low temperature to the freezing phenomenon of the super-cooled generated water where heat of solidification is emitted and the temperature rises to 0 °C.

Apparently, water becomes completely frozen at much lower temperatures than −10 °C. The study carried out by Saito et al. [281] suggest that even at temperatures below −20 °C the non-freezing water molecules remain unfrozen and move within the membrane. Their analysis was based on the estimation of the water self-diffusion coefficient, and on the differential scanning calorimetry (DSC) measurements that enabled the observation of the anomalous behaviour of non-freezing water. Interestingly, Mukundan et al. [282] detected at the extremely low temperature of −80 °C

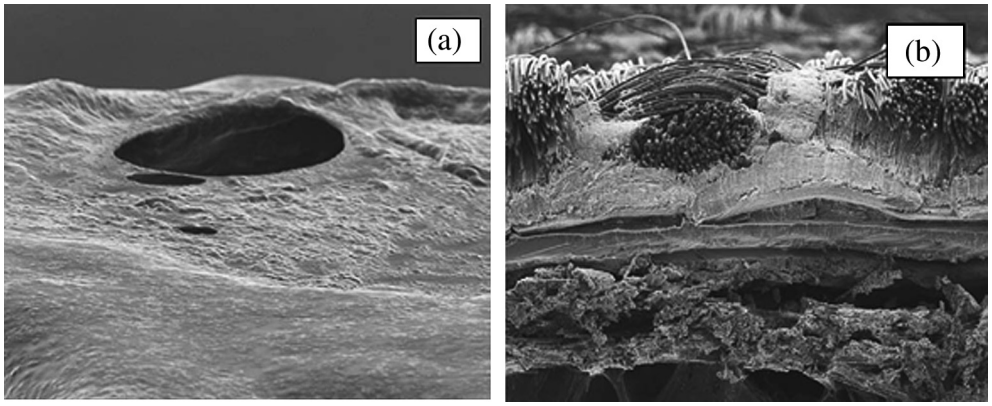


**Fig. 12.** Effect of sub-zero temperature on MEA after operation at −30 °C (a) pinhole formation on membrane from cathode outlet regions (b) catalyst delamination from GDL (Reproduced from Ref. [264] with permission).

interfacial failure in the cell suggesting possible freezing point of water in the cell.

The reduction of the water content due to ice formation clearly reduces the mobility of hydrogen ions across the membrane; a reduction in the ionic conductivity of the membrane is therefore expected. The experimental work of [284] showed how by decreasing the cell temperature to −25 °C, the water content of PFSA and BPSH membranes can be significantly reduced and the proton transport coefficients to become much less. Based on the measurements represented in Refs. [282,285], the membranes conductivity reduces substantially at subfreezing temperatures. The conductivity in Ref. [282] was reduced from 87 to 6 mS $cm^{-1}$ as temperature drops from +30 to −30 °C. Similar results were obtained by Koiwai et al. [285] as conductivity reduced from 100 to ∼1 mS $cm^{-1}$ with temperature dropping from 40 °C to −40 °C. According to Alink et al. [267], the decrease in membrane conductivity under sub-zero temperatures is attributed to membrane dehydration as a result of changes in the capillary pressure at the membrane/catalyst interface. They explained that during the heating process, the phase transition from ice to liquid water results in an increase of the capillary pressure leading to expansion of the membrane channels and increase of conductivity.

### 4.2. Water flooding

Flooding in PEMFC often occurs at high current densities when the generation rate of by-product water exceeds the removal rate of residual water from the cell. Flooding can be detected in-situ by either direct visualisation of the cell sub-layers or by monitoring the membrane's ohmic resistance. For example, as reported in Refs. [318], the change in the standard deviation of impedance measurements was an indication of flooding in PEMFC. Generally, measurements of membrane's impedance are carried out when optical accessibility to the cell is quite limited.

The sudden drop in the voltage level of the cell is another sign of flooding in PEMFC. The blockage by residual water of the access of reactant gases to the catalyst sites means the electrochemical reaction of the cell will stop. The sharp voltage decline takes place immediately after reaching the limiting current density of the cell better known as the cut-off current density. Many experimental studies have demonstrated this behaviour and attempted to extend this cut-off value which can be achieved by introducing advanced water management schemes to the cell.

Although many techniques have been used to detect flooding in PEMFC, optical visualisation techniques remain the most effective. Not only they help to identify key parameters that cause flooding, but also enable the anticipation of water flooding before happening. For example, the photographic images captured in Ref. [106] have allowed monitoring of the water build-up in the cathode flow channels. From those images, they were able to estimate how long it takes for a single PEMFC to be flooded with liquid water. As predicted after 30 min of operation, the channels were completely flooded followed by a significant drop in the cell current (e.g. 4.5 to 0.5 A). It is worth noting that almost all in-situ visualisation of water droplets on the surface of the membrane are made from the top view of the air flow channels which doesn't allow parameters such as droplets contact angles, droplets height, and droplets interfacial area with the surface to be estimated. However, it is possible to view droplet formation on the surface of the membrane from both the top and side view of the channels simultaneously as shown by Ous and Arcoumanis [140]. Fig. 13 illustrates the optical set-up used in Ref. [140] which consists of two synchronised cameras positioned orthogonally while Fig. 14 shows images of droplet formation on the surface of GDL at various locations in the air channels.

Water flooding does not only affect PEMFC performance but its durability too. This is due to the presence of excessive water that leaves the cell fuel starved and thus induces local potential on the

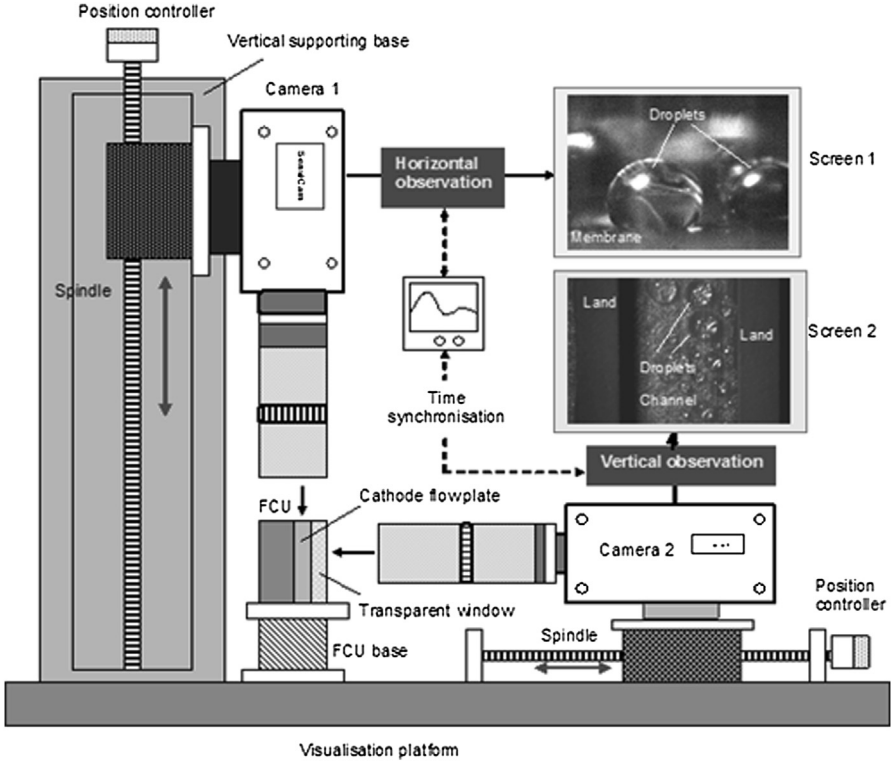


**Fig. 13.** Visualisation set-up [140].

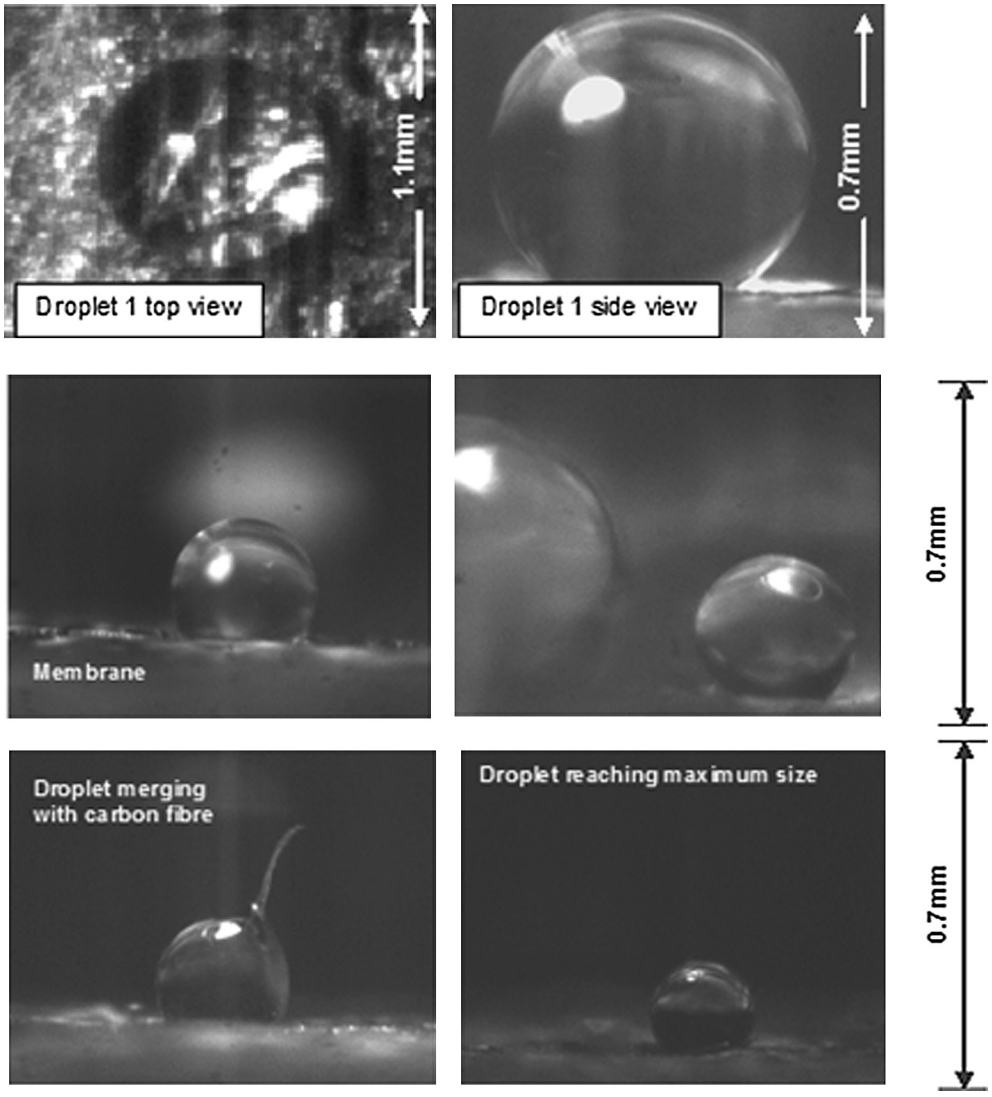


**Fig. 14.** Droplet formation on the surface of GDL at various locations in the cathode flow channels [140].

electrodes [319]. Reiser et al. [240] demonstrated both experimentally and numerically how local starvation of hydrogen can raise the cathode interfacial potential to as high as 1.44 V. At this high potential carbon corrosion of the catalyst can take place in just a few hours. The effect of this reverse-current mechanism was detected later by electron microprobe analysis (EMPA) images which showed significant decrease in the catalyst active surface area and thinning of the cathode electrode. Similarly when Patterson and Darling [194] restricted the access of hydrogen fuel to the cell by impregnating the anode GDL with kynar film, the cathode catalyst layer was severely corroded. Their EMPA images showed significant thinning of the cathode catalyst layer. Similar thinning of the cathode electrodes was observed by Liu et al. [195]. The thickness was reduced by as much as 60% in the $H_2$ starved region in comparison to the 10% reduction of the surrounding areas. Based on the limiting current density distribution map of their measured MEA, this $H_2$ starved region has also the lowest value of current density. Finally, the role of water flooding on carbon corrosion of the catalyst was further entrenched by Li et al. [320] who discovered after observing the MEA structure that carbon corrosion was more severe underneath the flow-plate lands where most water is expected to accumulate. Membrane thinning was in fact present in those under-land regions where thicknesses of 4 mm compared to 10 mm under the channels were observed.

### 4.3. Mitigation strategies

#### 4.3.1. Membrane swelling

Since swelling of polymer membranes is strongly dependant on their water content, it is plausible to operate the cell under less wet conditions. However, this will be at the expense of the ionic conductivity of the membrane which may cause greater decline in cell performance than what swelling would initiate. Controlling the access of external water to the cell through relative humidity can minimise the effect of swelling. The simulation of [286] showed how swelling stresses in the MEA become much higher with increasing RH. For example, the in-plane stresses in the membrane at a swelling strain of 0.05 were increased from 0 to 4 MPa as RH increases by only 10% (e.g. from 90 to 100% RH). Another model developed by Parrondo et al. [219] suggests that the compressive force applied during cell assembly affects membrane swelling. Since compromising with the operating conditions is unwise for the sake of cell performance, it could be more sensible to modify

instead the design of MEA and its assembly at an early stage to account for swelling.

Improving the mechanical and chemical properties of polymer membranes is probably the best approach to prevent swelling. A number of composite designs were developed in order to achieve minimal change in the membrane structure while keeping its conductivity at the highest level possible. Statterfield et al. [222] suggested the addition of Titanium oxide (titania) for improving the elastic and plastic deformation behaviour of Nafion under changes in temperature and water concentration. These composite membranes (e.g. Nafion–titania) exhibited less strain hardening than Nafion and resulted in 40% reduction in the membrane's creep compared to Nafion. Similarly, the focus in Ref. [222] was to improve the elastic modulus of Nafion 115 membranes by adding titania particles. This composite membrane showed after 3000 min of operation ~40% more reduction of creeping compared to extruded and recast Nafion types under the same stress conditions. The water uptake of these composite membranes was examined by means of resistivity measurements of the membrane which was reduced noticeably during the early stages of testing due to water absorption. Although the resistivity of Nafion/titania composites decreased slightly faster than the extruded Nafion with water absorption, these composite membranes still have lower resistance than Nafion.

The design developed by Ballengee and Pintauro [288] performed well against swelling. They used a composite of 70 vol% 660 equivalent weight perfluorosulfonic acid and 30 vol% polyphenylsulfone with the aim of conserving the dimensional stability of the member after water uptake. The in-plane swelling was increased by only 5% from the original size of the membrane at room temperature. Another sulfonated poly design was examined in Ref. [289] which contains sulfonic acid groups on aliphatic side chains. Although this design exhibited good protonic conductivity of around 0.11 S $cm^{-1}$, the swelling ratio was slightly higher than what was achieved in Ref. [287] (~12.9% at 100 °C). The difference between these two swelling ratios may be attributed to the degree of sulfonation applied during membrane preparation as pointed out by Reyna-Valencia et al. [234].

Various materials and preparation techniques were used in order to develop novel membrane designs that are capable of overcoming the effects of swelling. Parrondo et al. [219] suggested treating the polymeric matrix of membranes with acids and heat to improve the mechanical properties of polymer against changes in water activity. The intention was to decrease the elastic forces of the matrix and the swelling pressure so that the water content in the membrane remains relatively high. This design actually improves the water-uptake of polymer remarkably. A different approach was suggested in Ref. [287] for blending sulfonated polyethersulfone (SPES) based membranes with polyacrylonitrile (PAN) and polysulfone (PSU) composites. Their design was based on creating sulfone cross-linking groups between the polymer chains to bridge the arylsulfonic acid groups of SPES with the aryl groups in PSU. Their idea was to control the sulfonation level of SPES in order to improve the solubility of the material as well as to reinforce its structure. This design gave good results as the swelling ratio decreased by more than 70% while the drop in the membrane's conductivity was just 25%.

A new class of polymers, known as microblock ionomer, was developed by Zhu et al. [290] as a potential swelling-resistant membrane. The new design is based on sequence-distribution of sulphonic acid in ionomer backbone forming ionic and non-ionic spacer segments. This unique structure of phase-separation between hydrophilic and hydrophobic domains performed seemingly well against swelling. At a temperature of 120 °C, the ion exchange capability of the membrane was more than 2 meq $g^{-1}$.

Another approach to overcome swelling is to use gel-based membranes. These newly developed membranes are expected to be less susceptible to physical changes in aqueous solutions than traditional polymer membranes. Since their acidic structure (e.g. loosely bonded rather than formed within the polymer matrix) promotes protonic transport, their conductivity is not critically influenced by the hydration state or humidity of the reactant gases. The advantage of using this type of membrane becomes more pronounced at high operating temperatures where the majority of the water content in the membrane evaporates. Previous experimental studies [291–293] haven't reported any evidence of swelling of these gel membranes. Their focus was instead on the ionic conductivity and stability of these membranes under high temperature conditions. The measurements of [292] suggested that the conductivity of these membranes was around 0.01 S $cm^{-1}$ at 100 °C. Similar results were obtained by Ref. [293] but at the slightly higher temperature of 115 °C. The highest conductivity was reported in Ref. [293] where it reached a value of 0.1 S $cm^{-1}$ at room temperature and remained the same up to 85 °C.

#### 4.3.2. Corrosion

New materials were developed to prevent carbon corrosion in the catalyst layer of PEMFC [296,299,300]. The prime intention was either to improve the electrochemical stability of the carbon particles or to replace the carbon support with novel materials completely. It is worth noting that the type of carbon substrate used for the catalyst layer plays a key role in the carbon corrosion of PEMFC. Okada et al. [301] highlighted the advantages of using small surface area of carbon to support Pt particles in the catalysts. Graphitized carbon was the preferred option which showed improvements in catalyst durability and the overall performance of the cell. With this type of carbon, the amounts of Pt dissolution and $CO_2$ generated by the cell were quite small.

Carbon black is commonly used as a support for Pt catalysts in PEMFC. They offer a number of advantages that make them more attractive than other materials; this includes high porosity, high electrical conductivity, electrochemical stability, and nano size particles for the large active surface area of the catalyst.

Carbon black-supported Pt catalysts were previously examined in Refs. [210,294] against new designs of single and multi-walled carbon nanotubes (MWNT). The comparison was based on the change in Pt agglomeration and distribution at the catalyst surface after cell operation. Wang et al. [294] found only nominal reduction in Pt loss by around 37% under constant potential when MWNT was utilized as catalyst support compared to 80% of carbon black Vulcan CX-72. The reason for this large difference in the results was due to Pt migration and ripening/aggregation which were enhanced by the carbon corrosion of the catalyst. Similarly, the Pt loss in Ref. [210] was reduced by almost half under accelerated degradation testing, e.g. 43% with single-walled buckypaper compared to 80% loss with Pt/carbon. According to [210] the slow formation of surface oxides in the buckypaper design was the main reason for such a significant difference in the corrosion resistance.

The addition of Titania ($TiO_2$) to carbon-supported platinum catalyst (Pt/C–$TiO_2$ or Pt–$TiO_2$/C) was suggested by Selvaganesh et al. [297] and Sambandam et al. [298]. Both studies have agreed about the role of Titania in improving the performance and durability of PEMFC. The measurements in Ref. [297] showed lower degradation in cell performance of the Pt–$TiO_2$/C than the typical Pt/C catalyst. After 5000 test cycles, the degradation of Pt–$TiO_2$/C was 10% compared to 28% for Pt/C. The effect of $TiO_2$ was evident from the FESEM (Field Emission Scanning Electron Microscopy) images which showed higher deformation of the MEA structure with Pt/C catalyst in comparison to the Pt/$TiO_2$/C design. Similar results from their galvanostatic measurements were shown in Ref.

[298] indicating superior stability of Pt/C–$TiO_2$. By inserting the data from the electrochemical impedance spectroscopy spectra to a Randles equivalent circuit, Warburg element, and transmission line models, they were able to simulate $O_2$ transport and estimate the electrical resistivity of the catalyst. They found that Pt/C catalysts limit the flow of $O_2$ through the micro-porous structure of the electrode. This is mainly due to the increase in the catalyst layer thickness originating from the lower loading of Pt on the carbon support. Alternatively, Huang et al. [295] suggested replacing the carbon with Titania. Their analysis suggests that Pt/C catalyst suffered severe carbon corrosion, Pt dissolution, and catalyst particle sintering after 2000 potential cycles. Meanwhile, Pt/$TiO_2$ experienced only a small drop in voltage ($\sim$0.09 V at 0.8 A $cm^{-2}$) despite doubling the number of test cycles.

Metallic bipolar plates are the other components in PEMFC that are susceptible to corrosion. Various materials and coating techniques were utilized to avert corrosion of these plates including ferritic stainless steel (AISI446) [252]; metallic amorphous alloys ($Fe_{50}Cr_{18}Mo_8AL_2C_{14}B_6$) [302]; sulphuric acids ($H_2SO_4$) [250]; TiN coating by multi-arc ion plating [303]; stainless steel alloys (Fe–20Cr–4V) by thermal nitridation [304,307]; Polymer Polypyrrole and Polyaniline coating by cyclic voltammetry and painting [305]; and YZU001 like-diamond film by physical vapor deposition (PVD) [306]. The main focus has been on the polarisation characteristics of the cell but more specifically on the magnitude of ICR between the plates and the neighbouring carbon diffusion layers.

Lee et al. [306] were able to compare the contact resistance of coated aluminium, stainless steel (SS316L), and graphite plates as a function of the compaction force. The contact resistance of coated aluminium was smaller than that of the uncoated stainless steel resulting in better cell performance. At a constant cell voltage of 0.6 V, the current density of SS316L was 158 mA $cm^{-2}$ whereas for coated aluminium was 232 mA $cm^{-2}$. Graphite plates exhibited the best characteristics with the lowest contact resistance and slowest corrosion rate. Under 30 kg of applied compaction force, the contact resistance of SS316L, coated aluminium, and graphite plates after 4 h testing were 27, 25, and 15 mΩ, respectively. Jayaraj et al. [302] suggested using metallic amorphous bulk alloy ($Fe_{50}Cr_{18}Mo_8AL_2C_{14}B_6$) as a potential replacement of stainless steel for bipolar plates. They found this new alloy to be more resistant to corrosion than the stainless steel SS316L when tested in 1 M $H_2SO_4^{+2}$ ppm $F^-$ solution at 75 °C; the passive film formed on the surface was also found to be very stable.

In Refs. [304,305] concentration was focused more on reducing the interfacial contact resistance between the plates and the neighbouring GDL for maintaining optimum performance of the cell. Brady et al. [304] applied a new coating alloy (Fe–20Cr–4V) on stainless steel plates using nitridation and pre-oxidation treatments whereas in Ref. [305] aluminium plates were painted with Polyaniline. The coating method proposed in Ref. [305] proved to be effective since the increase in ICR value was still at an acceptable level, e.g. $\sim$0.3 Ω $cm^2$ above 200 N $cm^{-2}$ compressive force.

The increase in ICR due to the formation of a passive film at the interface between the corroded plates and the neighbouring GDL is directly proportional to the thickness of the film. Once the film stops developing, the value of ICR stabilises. Yang et al. [250] have suggested that a way to reduce the thickness of this n-type semiconductor film is to increase the concentration level of the sulphuric acid in the cell. This was their conclusion after they monitored the corrosion behaviour of SS316L bipolar plates in a simulated PEMFC cathode environment and at different sulphuric acid concentrations.

Another advantage of coating is to prevent the disassociation and dissolution of metallic cations such as $Fe^{3+}$, $Ni^{2+}$, $Cu^{2+}$, $Cr^{3+}$ that can potentially contaminate other parts of the cell and poison the polymer membrane and catalyst layers. The review conducted by Cheng et al. [308] highlighted the danger of small quantities of these impurities in damaging the anode, membrane, and cathode chemical properties and causing a drop in cell performance.

#### 4.3.3. Ice formation

Numerous techniques can be applied to prevent ice formation from deteriorating the performance and lifetime of PEMFC [273,283]. One way to achieve this is to introduce heat to the cell in order to maintain its thermal state above freezing. Sun et al. [309], for example, suggested generating heat by mixing hydrogen and oxygen gases in the cathode channels to enable for catalytic hydrogen reaction. This method did not cause drop in cell performance and it was also safer to operate having the concentration of hydrogen not exceeding 40% of the total gas mix ($H_2/O_2$). Apparently, this method has enabled the temperature of the cell to be raised from cold start condition of −20 °C to 0 °C in 6 min with only a 20% hydrogen concentration.

Ge and Wang [274] were also able to increase the cell temperature to as high as 70 °C and at the same time avoid significant Pt reduction from the active surface area of the catalyst. The trapped liquid water between Pt particles and ionomers in the cathode catalyst layer under −30 °C cold-start caused the surface area to decrease by around 35% (e.g. $\sim$73 to 47 $m^2$ $g^{-1}$). According to the current and temperature distribution measurements of [310], the highest current density during failed cold start is occurring initially towards the reactant inlet regions of the cell; around 40–50% of the total cell current is produced in these regions. This finding suggests that it is more effective to apply external heat to the inlet rather than to other regions of the cell.

Purging the cell with dry gases is another method to overcome the effect of ice formation. The concept is to remove liquid water from the cell before it is transformed into ice at subfreezing temperatures. However, this process has to be repeated every time the cell is out of operation, i.e. it shuts down. Experimentalists tend to disagree about the duration needed for purging to achieve successful cold start operation of the cell. For example in Ref. [278], a duration of 120 s is suggested to be sufficient whereas in Ref. [310] much longer period of 2 h is recommended. Obviously the purging duration will be dependant on the design of the cell and its operating condition. Ge and Wang [278] showed the effect of purging time on the amount of water extraction from the membrane and how it improves the performance of the cell. This was again confirmed in [256] when they compared the performance of the cell with and without purging under a temperature of −10 °C. Despite the fact that the measurements were carried out at a low current density ($\sim$0.15 A $cm^{-2}$), the current density dropped significantly without purging after just 15 s of operation. In contrast, the duration until failure was extended to 268 s when purging was used.

One of the main advantages of purging is to protect the PEMFC components from structural damages by subfreezing temperatures. The purging used in Ref. [260] was sufficient to maintain the catalyst structure unchanged under temperature cycles of −30 °C in comparison to the damage with the non-purging condition as illustrated in Fig. 10. The impact of purging is not only on the durability of PEMFC but on its performance as well. In Refs. [264], the cell failed to operate even at −5 °C and at a low current density of no more than 200 mA $cm^{-2}$ when purging was not employed. The free water, which is expected to be trapped at the catalyst layer, can freeze hindering the access of reactants to the reaction sites of the catalyst and causing a performance drop.

It is important to set the relative humidity of the purging gases to a medium level, neither too dry nor too wet. Otherwise the cell can suffer from poor ionic conductivity of the reduced water

amount in the membrane or from water flooding at the early stages of subsequent operating cycles. When Hou et al. [311] increased the relative humidity of the purging gas from 16.6% to 64.9%, although no performance loss was detected after 20 freeze/thaw cycles, the flow channels were completely flooded with liquid water in the first cycle at high current density (1 A $cm^{-2}$). Consequently, the MEA was more damaged at −30 °C with an increase from the initial porosity by 10% compared to 2% of the drier purge gas.

Other parameters such as purging time, gas flow rate, cell current and temperature also determine how effective the purging process is. One may expect that if purging is happening quite frequently or for long duration, the cell membrane would dehydrate more easily. In fact, in Ref. [312] was shown that, for purging the cell, high flow rates and temperatures are the most influential factors. They examined different purging scenarios and found that raising the flow rate of the purging gas extracts more water than extending the purging duration for the same amount of purge gas. Furthermore, purging at ambient temperatures is inefficient.

Four gases have been mainly used for purging in PEMFC including air, $H_2$, $O_2$, and $N_2$; each of these gases performs differently. When Gavello et al. [313] tried purging the cell with $N_2$, air and $H_2$ gases, they found that the best combination is to use dry air and dry $H_2$ at the cathode and anode, respectively. With this purging strategy, MEAs exhibit the smallest loss in power density and minimal damage of their structure (e.g. loss of 7.6% after 20 Freeze/Thaw cycles and 19.3% after 30 cycles). The only disadvantage was that it encourages strong migration of Pt particles from the catalytic layer towards the membrane. Alternatively, Cho et al. [315] tried purging the anode with dry $N_2$ and the cathode with $O_2$. The performance degradation rate of the cell was significantly reduced from 2.3% to 0.06%, and the reduction in Pt utilisation of the catalyst was also very small (∼3% during 7 testing cycles). Song and Kim [314] suggested purging only the cathode with dry air but not the anode since the damage of freezing on the anode is quite small; they tested various purging schemes and operating conditions to assess their effects in terms of Pt loss from the catalyst surface area and the mass transfer limitation. Purging the cell with antifreeze solutions is another alternative to the dry gas approach. Cho et al. [315] used 30% methanol and 35% ethylene glycol solutions for purging and by doing so the performance degradation rate of the cell was reduced to −0.16% and 0.47%, respectively.

Other researchers relied instead on improving the design of MEA against freeze/thaw degradation cycles. For example, Saito et al. [281] suggested using membranes with low equivalent weight (EW) values and high amount of freezing water (e.g. weakly interacting water with ionic groups) in order to enhance the $H^+$ conductivity. Wang et al. [316] employed multi-walled carbon nanotubes (MWCNTs) to reinforce Nafion resin for enhancing the mechanical stability and tensile strength of the membrane. The increase in the $H_2$ oxidation current density of MWCNT-reinforced Nafion membrane was eventually lower compared to Nafion-112 (71% vs 109%). Song et al. [317] added isopropyl alcohol and isopropyl butyl acetate to the catalytic ink of catalyst-coated membrane. These two designs not only improved the ionic resistance of the membrane but also exhibited less degradation in terms of the electrochemical active surface area and polarisation curves of the cell.

#### 4.3.4. Flooding

The best way to avoid water flooding in PEMFC is probably to operate the cell under conditions which allow effective water extraction from the cell. Obviously operating the cell under low current densities minimises the risk of flooding, as a result of the proportional relationship between cell current and by-product water; thus water management becomes less of an issue. Nevertheless, increasing the temperature of the cell has two main advantages. First, it allows rapid evaporation of the residual water in the cell, thus preventing further water accumulation, and also it enhances the kinetics of the catalyst.

Ous and Arcoumanis [106] estimated the amount of water that can be removed from a single PEM cell for each 1deg temperature rise (∼34 nl $°C^{-1}$). Their in-situ visualisation of the cathode and anode flow channels showed that water disappears completely from the channels as the temperature reaches 60 °C. The same happened when they increased the air flow rate to the high stoichiometry of 36 where water droplets on the surface of the channels were all blown away. Their measurements also suggest that, on average, temperature has a higher extraction rate of liquid water from the flow channels of the cell than stoichiometric air (∼34 nL °C vs. 26 nL $°C^{-1}$). However, both of these operating parameters should not be excessive otherwise the membrane could become fully dehydrated.

An alternative method to prevent flooding in PEMFC is to use materials that can improve the transport of liquid water in the cell [259]. For instance, loading the catalyst or GDL with hydrophobic substances such as polytetrafluoroethylene (PTFE) helps to expel excess water from the void regions of these layers. Oh et al. [321] have suggested moderate addition of copolymer P (VdF–Co–HFp) to the catalyst layers in order to improve the hydrophobic characteristics of catalysts and suppress water flooding. The improvement in the hydrophobicity of the catalyst was evident from the contact angle measurements of water droplets on the surface. These measurements showed a noticeable angle increase with added copolymer, e.g. contact angles were 36°, 86° and 105° with copolymer loading of 0, 2–5 and 10 wt.%, respectively. The performance of the cell was enhanced both in terms of current density and ohmic resistance of the catalyst. However, excessive loading proved detrimental to the polarisation performance. When copolymer loading was increased from 5 to 10 wt%, the current density of the cell dropped from 530 to 484 mA $cm^{-2}$. The addition of oxygen permeable and hydrophobic dimethyl silicone oil (DSO) to the catalyst layer was also suggested by Li et al. [80] in order to improve the water balance and oxygen accessibility to the catalyst cathode. Again, the hydrophobicity of the catalyst was increased remarkably with the addition of only 0.5 mg $cm^{-2}$ of DSO, as evidence by the improvement in the limiting current density of the cell which was extended from 1.2 to 2 A $cm^{-2}$.

Lin and Nguyen [322] stated that the cell can still operate with maximum gas and water transport mechanisms during flooding with a moderate addition of PTFE to GDL. When they compared the performance of the cell with different PTFE loading of Toray carbon paper (10, 20, and 30% PTFE), the paper with the medium PTFE content (e.g. 20%) showed the best performance. They argued that combination of hydrophobic pores for gas transport and hydrophilic pores for liquid water transport can give GDLs the ultimate design configuration against water flooding.

## 5. Water transport in PEMFC

Water in PEMFC originates from two main sources. It is either produced by ORR at the catalyst cathode or fed externally into the cell through the humidification or cooling gases. The amount of by-product water can be calculated directly from the current density of the cell. The amount of external water is, however, more difficult to estimate since it varies depending on the temperature, pressure and flow rate of the humid/coolant gas used.

In general, water transport in PEMFC involves a complex interplay of processes. In the membrane, for example, there are three water fluxes during the operation of the cell known as electro-osmotic drag, back diffusion and water generation. The effect of

electro-osmotic drag on the water distribution is considered to be the dominant as many hydrogen ions drag water molecules when travelling from the anode to cathode. Meanwhile, the high concentration of the water generated at the cathode forces the water stream to diffuse back into the anode. The balance between these two fluxes is critical for maintaining a uniform water distribution across the membrane and hence an optimum ionic conductivity of the membrane. The effect of back diffusion becomes more significant at high current densities and particularly when the extraction rate of water from the cathode region is extremely low.

### 5.1. MEA and GDL structure

Various models [323–327] have been developed to simulate water transport mechanisms across polymer type membranes. The aim is to estimate the water diffusion rate during the operation of PEMFC including parameters like water transport and electro-osmotic drag coefficients (e.g. the water transport coefficient is defined as the ratio of net water flux across the membrane to water production, whereas the drag coefficient is the number of water molecules transported per proton). Interestingly enough, one of these models e.g. Ref. [324] is suggesting that ageing has no influence on the water transport coefficient despite other studies [32,219–223,227,228] where a significant change in the physical properties of aged membranes was detected. However, none of these studies have addressed the effect of water transport mechanism on membrane durability. This effect was rather related by other experimental and modelling investigations to the relative humidity condition of the cell.

Since increasing the RH of the reactant gases increases the rate of water flux across the membrane layer [324,328] and results in higher release of fluoride ions from those membranes [30,74,329,330], water transport in the membrane is expected to play a part in the fluoride emission of PEMFC. Water transport may also affect some of the mechanical, electrical, and chemical properties of the MEA like the porosity of GDL, polymer chains, and Pt distribution in the catalyst. The simulations carried out by Lin and Nguyen [231] showed how, by increasing the relative humidity of the reactant gases, the polymer chains in the membranes become more susceptible to unzipping.

The results presented in Ref. [30] showed an increase in the concentration level of fluoride ions by more than 3× (∼450 ppb) after 800 h under highly water saturated operation (e.g. air humidity is 100% and hydrogen >100% RH). They suggested that the main cause for this was the water generated and the inlet water flow which could wash away the recast ionomer from the cathode catalyst continuously. Under the same humidity but slightly higher Nafion membrane loading (e.g. 100% RH at 33 wt % Nafion), Young et al. [197] detected fluoride loss of around 25% after 440 h of AST (60 μmol $cm^{-2}$ from total MEA content of 230 μmol $cm^{-2}$). Uchida et al. [329] also found that, increasing the relative humidity of mixed gases ($H_2$ + 10% air, air +2% $H_2$), increases the fluoride emission rate (FER) almost linearly. Raising RH from 0 to 90%, the FER using $H_2$ + 10% air mixture increases from 3.5 to 10 nmol $h^{-1}$ whereas for air +2% $H_2$ mixture the range of increase was from 1.25 to 7 nmol $h^{-1}$.

Apparently, fluoride emission rate does not only increase at the high RH operation but under low humidity conditions too. Kundu et al. [200] detected significant loss of fluoride, by around 45%, when RH was reduced from 100% to 20% (e.g. from ∼29 to 52 μmol $cm^{-2}$). Again, the comparison made in Ref. [231] between different humidity conditions (e.g. 82%, 55%, and 36% RH) revealed much higher FER values at humidity levels lower than 50%.

The dissolution of Pt particles from the active surface area of the catalyst layer due to the increase in the RH of the reactant gases was reported previously in Refs. [241,332]. Uchimura et al. [241] found that the active surface area of the catalyst reduces dramatically by around 50% when RH increases from 30 to 100%. Furthermore, they claimed that if the membrane can survive low RH conditions, the dissolution of Pt particles would be significantly diminished. The reason for Pt dissolution at high RH conditions could be attributed to the enhanced ORR activity of the catalyst at the high hydration state of the membrane. It may also be due to water flooding which can cause fuel starvation in the cell and induction of a local potential on the electrodes [194,195,240,242].

Migration of $Pt_3Cr$ alloy particles from the catalyst layers under fully humidified conditions was observed in Refs. [30,192]. Xie et al. [30] presented images showing chromium particles accumulated in the anode catalyst layer. One possible explanation for this is that the high current density they operated at (>1 A $cm^{-2}$) has generated excessive water facilitating chromium particles to be carried away by the back diffusion stream to the anode. Similarly, the Pt migration detected in Ref. [332] was found to be more severe at the cathode layer than the anode. When the cell was operated with three different levels of cathode inlet RH (e.g. 0, 50, and 100%) for 1500 cycles, the highest Pt loss from the catalyst cathode was at 100% RH [332]. According to their analysis, this was attributed to the corrosion of the carbon support which intensifies at higher RH.

The partial pressure of $H_2$ and $O_2$ tends to influence the distribution of Pt particles according to the simulations of [196]. Their model showed how relative local flux of $H_2$ and $O_2$ determines the location of Pt repositioning. This was validated by SEM images which revealed the formation of a Pt band closer to the anode or cathode catalyst layers depending on the operation pressure ratio of the reactant gases. For example, when the $H_2/O_2$ pressure was reduced to 20%, the Pt band appeared near to the anode catalyst layer (e.g. away by 4.3 μm) rather than near to the cathode/membrane interface when the pressure ratio is equal. In Ref. [192] the migration of $Pt_3Cr$ particles was from both electrodes towards the membrane and in addition, they found that pure Pt particles are more susceptible to migration than $Pt_3Cr$ alloy due to their electrochemical instability. This was concluded after observing that stronger migration is taking place at the pure-Pt anode catalyst.

The mechanical properties of GDL should also be affected by the water transport mechanism in PEMFC. Numerical simulations of the water transport through different types of GDL were carried out in numerous investigations [333–347]. The majority of these two- and three-dimensional models suggest that the transport of liquid water through GDL is mainly dominated by the hydrophobic and morphological properties of the GDL including porosity, tortuosity, cross sectional area, thickness, and PTFE loading. Other design and operating factors such as the compaction force used for the cell assembly [124], operating temperature [335], stoichiometric ratio of reactant gases [336], and GDL wettability [337,342] were also found to affect water diffusion in the GDL. It is expected that the more the water diffuses through the layer, the more the damage on the GDL structure can be. However, still more research work needs to be done in this area to understand this effect in depth.

### 5.2. Contamination

The effect of relative humidity on the degradation of PEMFC was previously associated to a number of factors such as membrane swelling [220,228], membrane thinning [229,230], creep formation and cracking [73,231], fluoride concentration change [30,74,200, 330,331], catalyst particles migration [67,68], carbon corrosion [48,69,241], pin-hole formation [32,227,228,232], hydrogen cross-over [36,44,74] and local fuel starvation [194,195,240,242].

Equally damaging as these factors is the kind of water used for the humidification of the reactant gases. Drinking water contains

harmful contaminants such as Fe, Cu, Cr, Si, and Al that can potentially poison the MEA and cause performance decay of the cell. The concentration level of the contaminants determines the deterioration rate of the MEA. In Refs. [348], Fe concentration was initially less than 1 ppm in their tested GORE-SELECT membrane. The level of Fe increased dramatically when external water was added to the cell under humid-air operation as evident from their MEA durability measurements which revealed higher fluoride release rate (FRR) than in the case of the cathode running with dry air (e.g. 1.6E-08 vs. 1.5E-07 g $cm^{-2}$ $h^{-1}$).

The corrosion of fuel cell stack components like metal bipolar plates, end plates or humidifier reservoir is another source of impurities. Liquid water may carry traces of metal ions such as $Fe^{+2}$ and $Cu^{2+}$ to the MEA causing permanent defects to its electrical, mechanical, and chemical properties. The review of [308] highlighted the effects of these impurities on cell performance which were found to be detrimental particularly in terms of the cell electrode kinetics, conductivity, and mass transfer.

Probably the best example to demonstrate the role of water in transporting these harmful contaminants is from the experimental work of Pozio et al. [349]. When they used two different end plates in the cell, e.g. stainless steel SS316L and aluminium Al, they discovered significant difference in fluoride release under the same testing conditions (14 ppm for SS316L vs. 1.2 ppm for Al). The pH level of water collected at the anode and cathode for SS316L was around 30% lower than in the case of the Al plate. Clearly the water was the primary agent for revealing such differences and transporting traces of contaminants.

### 5.3. Mitigation strategies

The effect of water transport on the degradation of PEMFC can be minimised if the amount of water moisture in the cell is kept small. However, as explained before in Section 4.3, this has a dramatic impact on membrane conductivity and cell performance. The best solution could be to maintain the hydration level in the cell but reinforce the design of MEA to withstand levels of deterioration originating from the water transport mechanisms.

A number of composite membranes were developed in order to improve the electrochemical stability of MEA. Trogadas et al. [350] added $CeO_2$ nanoparticles into Nafion membranes to reduce the fluoride emission rate from both electrodes. Without compromising in terms of proton conductivities and hydrogen crossover of the cell, the rate was lowered by more than one order of magnitude compared to a typical Nafion membrane (e.g. from 0.1 to 0.01 μmol $h^{-1}$ $cm^{-2}$). Inaba et al. [44] also suggested introducing an anti-gas crossover layer, a peroxide decomposition layer and $Fe^{2+}$ ion-trap layer into the MEA design in order to prevent oxygen crossover and consequent formation of hydrogen peroxide and catalytic combustion at the anode. In addition, as mentioned in Section 3.2, the MEA stability can be enhanced by impregnating the catalyst layer with alloys such as titanium [201], cobalt [187,202], aluminium oxide [212], titanium dioxide [213], zirconium dioxide [214] and tin dioxide [215].

Some other composites were designed specifically to operate under low RH conditions [34,85]. Su et al. [85] used $Pt/SiO_2/C$ for the anode catalyst aiming to achieve acceptable polarisation performance of the cell at low RH values. Indeed, the voltage and current density of their design cell (0.6 V, 0.65 A $cm^{-2}$) remained almost unchanged despite the significant drop in RH level at both the anode and cathode (e.g. RH reduced from 100% to 28%). Similarly, the Nafion–Teflon–phosphotungstic acid (NTPA) design of [34] had a marginal drop in cell voltage (~90 mV) at the low RH values of 25%. It is worth noting that operating the cell at low RH using these types of self-humidifying membranes offers two advantages in terms of PEMFC durability. First, it reduces the number of hydration/dehydration cycles during the life span of the cell which often lead to mechanical failures of the MEA. The second advantage is minimising the risk for foreign particles to access the cell with humidified gases and cause damage to the MEA.

Finally, PEMFC membranes are chemically fragile. The quality of the water used in the humidification process of the reactant gases is another important requirement for achieving durable cells. Deionised water is preferable since no ionic impurities are present. However, in case impurities are introduced from other external sources, such as a humidifier reservoir or other cell components, installing a filtration system at the inlet of the cell would probably be the most effective way to reduce or even eliminate the effect of these impurities.

## 6. Concluding remarks

The water management system does not only affect PEMFC performance but also its durability. A number of degradation factors such as the loss of active surface area of the catalyst, ionomer dissolution, corrosion, contamination, and morphological damages of MEA and GDL were identified which are influenced by water formation, retention, accumulation and transport mechanisms within the cell.

It is difficult to determine accurately the impact of each of these water mechanisms on the deterioration rate of the cell as it varies depending on the design and the operating conditions of the cell. For example, the effect of water retention and accumulation becomes more severe when the cell operates at subfreezing temperatures. The volume expansion of liquid water due to the ice formation causes morphological damages to different parts of the cell which can accelerate the degradation process. Furthermore, the effect of these water mechanisms on cell durability can be classified into two main categories: ageing and catastrophic. With ageing, durability and performance behaviour of the cell tend to decline steadily over time whereas in the case of catastrophic ones the cell fails instantly.

The role of water formation has been considered to fall into the 'aging' category as the loss of Pt active surface area and ionomer dissolution of the MEA happen interchangeably. A similar classification applies to the effect of water retention, accumulation and transport where changes in MEA and GDL properties including membrane swelling, porosity, corrosion of carbon catalyst support and metallic bipolar plates occur during the life-time of PEMFC. Only two factors, such as the formation of cell residual water into ice at subfreezing temperatures and the access of foreign contaminants by external humidification, are classified as catastrophic. These factors can lead to serious consequences such as membrane poisoning and catalytic combustion which cause an immediate termination of the PEMFC operation.

In conclusion, the effect of water mechanisms on PEMFC degradation can be minimised or even eliminated by (a) using advanced materials particularly for MEA and GDL to improve their stability (b) implementing effective strategies for extracting residual water from the cell, and (c) ensuring contamination-free operation of the cell to prevent poisoning of the membrane.

## Nomenclature

| | |
|---|---|
| ADT | accelerated durability test |
| AST | accelerated stress test |
| BPP | bipolar plate |
| BSEM | back scattered Electron Microscopy |
| CL | catalyst layer |
| CNF | carbon nanofibers |

| | |
|---|---|
| CNT | carbon nanotubes |
| DOE | department of energy |
| DSC | differential scanning calorimetry |
| DSO | dimethyl silicone oil |
| DWNT | double-walled nanotubes |
| EDX | energy dispersive X-ray |
| EMPA | electron microprobe analysis |
| ESEM | environmental scanning electron microscopy |
| EW | equivalent weight |
| GDBL | double micro porous layer |
| GDL | gas diffusion layer |
| GMPL | graded micro porous layer |
| HFP | European hydrogen and fuel cell technology platform |
| HOR | hydrogen oxidation reaction |
| ICR | interfacial contact resistance |
| FEP | ethylene propylene |
| FER | fluoride emission rate |
| FESEM | field emission scanning electron microscopy |
| FRR | fluoride release rate |
| M | membrane |
| MEA | membrane electrode assembly |
| MPL | micro porous layer |
| MVM | mean value model |
| MWNT | multi-walled carbon nanotubes |
| NEDO | new energy and industrial technology development organisation |
| NTPA | nafion–teflon–phosphotungstic acid |
| ORR | oxygen reduction reaction |
| PAN | polyacrylonitrile |
| PEMFC | proton exchange membrane fuel cell |
| PFSI | perflurosulfonate ionomer |
| PSU | polysulfone |
| PTFE | polytetrafluoroethylene |
| PVD | physical vapor deposition |
| RH | elative humidity |
| SEM | scanning electron microscopy |
| SPES | sulfonated polyethersulfone |
| SWNT | single-walled nanotubes |
| TEM | transmission electron microscopy |
| $\lambda_{air}$ | air stoichiometry |

## References


[1] W.G. Colella, R.J. Timme, J. Brouwer, N.M. Sammes, Journal of Power Sources (2011). in press, accepted manuscript.
[2] Jason Marcinkoski, Brian D. James, Jeff A. Kalinoski, Walt Podolski, Thomas Benjamin, John Kopasz, Journal of Power Sources 196 (12) (2011) 5282–5292.
[3] N. Rajalakshmi, K.S. Dhathathreyan, International Journal of Hydrogen Energy 33 (20) (2008) 5672–5677.
[4] Ashkan Esmaeilifar, Soosan Rowshanzamir, Mohammad H. Eikani, Ehsan Ghazanfari, Electrochimica Acta 56 (1) (2010) 271–277.
[5] Seunghee Woo, In Kim, Jae Kwang Lee, Sungyool Bong, Jaeyoung Lee, Hasuck Kim, Electrochimica Acta 56 (8) (2011) 3036–3041.
[6] S. Martin, P.L. Garcia-Ybarra, J.L. Castillo, International Journal of Hydrogen Energy 35 (19) (2010) 10446–10451.
[7] Roswitha Zeis, Anant Mathur, Greg Fritz, Joe Lee, Jonah Erlebacher, Journal of Power Sources 165 (1) (2007) 65–72.
[8] M. Prasanna, E.A. Cho, H.-J. Kim, T.-H. Lim, I.-H. Oh, Sung-Ahn Hong, Journal of Power Sources 160 (1) (2006) 90–96.
[9] Yuan Yuan, Joshua A. Smith, Gabriel Goenaga, Di-Jia Liu, Zhiping Luo, Jingbo Liu, Journal of Power Sources 196 (15) (2011) 6160–6167.
[10] H. Perez, A. Morin, L. Akrour, C. Cremona, B. Baret, J. Haccoun, S. Escribano, A. Etcheberry, Electrochimica Acta 55 (7) (2010) 2358–2362.
[11] R.K. Ahluwalia, X. Wang, J. Kwon, A. Rousseau, J. Kalinoski, B. James, J. Marcinkoski, Journal of Power Sources 196 (10) (2011) 4619–4630.
[12] Bin Wang, Journal of Power Sources 152 (2005) 1–15.
[13] Paolo Agnolucci, International Journal of Hydrogen Energy 32 (15) (2007) 3526–3544.
[14] Greg Frenette, Daniel Forthoffer, International Journal of Hydrogen Energy 34 (9) (2009) 3578–3588.
[15] Tasneem Abbasi, S.A. Abbasi, Renewable and Sustainable Energy Reviews 15 (6) (2011) 3034–3040.
[16] Andreas Pastowski, Thomas Grube, Energy Policy 38 (10) (2010) 5382–5387.
[17] F. Markert, S.K. Nielsen, J.L. Paulsen, V. Andersen, International Journal of Hydrogen Energy 32 (13) (2007) 2227–2234.
[18] Vivek P. Utgikar, Todd Thiesen, Technology in Society 27 (3) (2005) 315–320.
[19] U. Schmidtchen, Encyclopedia of Electrochemical Power Sources (2009) 519–527.
[20] R.K. Ahluwalia, T.Q. Hua, J.-K. Peng, S. Lasher, K. McKenney, J. Sinha, M. Gardiner, International Journal of Hydrogen Energy 35 (9) (2010) 4171–4184.
[21] Jinyang Zheng, Xianxin Liu, Ping Xu, Pengfei Liu, Yongzhi Zhao, Jian Yang, International Journal of Hydrogen Energy 37 (1) (2012) 1048–1057.
[22] S.W. Jorgensen, Current Opinion in Solid State and Materials Science 15 (2) (2011) 39–43.
[23] R.S. Gemmen, C.D. Johnson, Journal of Power Sources 159 (1) (2006) 646–655.
[24] Yun Wang, Ken S. Chen, Jeffrey Mishler, Sung Chan Cho, Xavier Cordobes Adroher, Applied Energy 88 (4) (2011) 981–1007.
[25] M. Marrony, Encyclopedia of Electrochemical Power Sources (2009) 297–308.
[26] R. Lin, B. Li, Y.P. Hou, J.M. Ma, International Journal of Hydrogen Energy 34 (5) (2009) 2369–2376.
[27] M. Marrony, R. Barrera, S. Quenet, S. Ginocchio, L. Montelatici, A. Aslanides, Journal of Power Sources 182 (2) (2008) 469–475.
[28] J. Zhang, R.N. Carter, P.T. Yu, W. Gu, F.T. Wagner, H.A. Gasteiger, Encyclopedia of Electrochemical Power Sources (2009) 626–638.
[29] S.-Y. Ahn, S.-J. Shin, H.Y. Ha, S.-A. Hong, Y.-C. Lee, T.W. Lim, I.-H. Oh, Journal of Power Sources 106 (1–2) (2002) 295–303.
[30] Jian Xie, L. David Wood III, David M. Wayne, Thomas A. Zawodzinski, Plamen Atanassov, Rodney L. Borup, Journal of The Electrochemical Society 152 (1) (2005) A104–A113.
[31] J. Scholta, N. Berg, P. Wilde, L. Jörissen, J. Garche, Journal of Power Sources 127 (1–2) (2004) 206–212.
[32] J. Yu, T. Matsuura, Y. Yoshikawa, M.N. Islam, M. Hori, Electrochemical and Solid-State Letters 8 (3) (2005) A156–A158.
[33] Michael W. Fowler, Ronald F. Mann, John C. Amphlett, Brant A. Peppley, Pierre R. Roberge, Journal of Power Sources 106 (1–2) (2002) 274–283.
[34] H. Xu, M. Wu, Y. Liu, V. Mittal, R. Vieth, H.R. Kunz, L.J. Bonville, J.M. Fenton, Electrochemical Society Transactions 3 (1) (2006) 561–568.
[35] Chih-Wei Lin, Chi-Hui Chien, Jinzhu Tan, Yuh J. Chao, J.W. Van Zee, Journal of Power Sources 196 (4) (2011) 1955–1966.
[36] Feng-Yuan Zhang, Suresh G. Advani, Ajay K. Prasad, Mary E. Boggs, Shawn P. Sullivan, Thomas P. Beebe Jr., Electrochimica Acta 54 (16) (2009) 4025–4030.
[37] Shengsheng Zhang, Xiao-Zi Yuan, Jason Ng Cheng Hin, Haijiang Wang, K. Andreas Friedrich, Mathias Schulze, Journal of Power Sources 194 (2) (2009) 588–600.
[38] Yongtaek Lee, Bosung Kim, Yongchan Kim, Xianguo Li, Journal of Power Sources 196 (4) (2011) 1940–1947.
[39] Jinfeng Wu, Jonathan J. Martin, Francesco P. Orfino, Haijiang Wang, Colleen Legzdins, Xiao-Zi Yuan, Colin Sun, Journal of Power Sources 195 (7) (2010) 1888–1894.
[40] Junhyun Cho, Taehun Ha, Jaeman Park, Han-Sang Kim, Kyoungdoug Min, Eunsook Lee, Jy-Young Jyoung, International Journal of Hydrogen Energy 36 (10) (2011) 6090–6098.
[41] Christoph Hartnig, Thomas J. Schmidt, Electrochimica Acta 56 (11) (2011) 4237–4242.
[42] Y. Hung, H. Tawfik, D. Mahajan, Journal of Power Sources 186 (1) (2009) 123–127.
[43] Adam Z. Weber, Journal of The Electrochemical Society 155 (6) (2008) B521–B531.
[44] Minoru Inaba, Taro Kinumoto, Masayuki Kiriake, Ryota Umebayashi, Akimasa Tasaka, Zempachi Ogumi, Electrochimica Acta 51 (26) (2006) 5746–5753.
[45] Wei-Mon Yan, Hsin-Sen Chu, Meng-Xi Lu, Fang-Bor Weng, Guo-Bin Jung, Chi-Yuan Lee, Journal of Power Sources 188 (1) (2009) 141–147.
[46] Georgeta Postole, Aline Auroux, International Journal of Hydrogen Energy 36 (11) (2011) 6817–6825.
[47] A.A. Kulikovsky, H. Scharmann, K. Wippermann, Electrochemistry Communications 6 (1) (2004) 75–82.
[48] L.J. Rod, John R. Davey, Fernando H. Garzon, David L. Wood, A. Michael, Journal of Power Sources 163 (1) (2006) 76–81.
[49] A.D. Modestov, M.R. Tarasevich, V.Ya. Filimonov, N.M. Zagudaeva, Electrochimica Acta 54 (27) (2009) 7121–7127.
[50] Héctor R. Colón-Mercado, Branko N. Popov, Journal of Power Sources 155 (2) (2006) 253–263.
[51] Karel Bouzek, Martin Paidar, Jakub Mališ, Ivo Jakubec, Luděk Janík, Electrochimica Acta 56 (2) (2010) 889–895.
[52] Mei Cai, Martin S. Ruthkosky, Belabbes Merzougui, Swathy Swathirajan, Michael P. Balogh, Se H. Oh, Journal of Power Sources 160 (2) (2006) 977–986.
[53] Jinfeng Wu, Xiao Zi Yuan, Jonathan J. Martin, Haijiang Wang, Jiujun Zhang, Jun Shen, Shaohong Wu, Walter Merida, Journal of Power Sources 184 (1) (2008) 104–119.

[54] Xiao-Zi Yuan, Shengsheng Zhang, Haijiang Wang, Jinfeng Wu, Jian Colin Sun, Renate Hiesgen, K. Andreas Friedrich, Mathias Schulze, Andrea Haug, Journal of Power Sources 195 (22) (2010) 7594–7599.
[55] Gilles Meyer, Gérard Gebel, Laurent Gonon, Philipe Capron, Didier Marscaq, Catherine Marestin, Régis Mercier, Journal of Power Sources 157 (1) (2006) 293–301.
[56] Yuyan Shao, Geping Yin, Yunzhi Gao, Pengfei Shi, Journal of The Electrochemical Society 153 (6) (2006) A1093–A1097.
[57] J. Zhang, K. Sasaki, E. Sutter, R.R. Adzic, Science 315 (2007) 220–222.
[58] Zhi-yong Xie, Gu-yin Jin, Min Zhang, Zhe-an Su, Ming-yu Zhang, Jian-xun Chen, Qi-zhong Huang, Transactions of Nonferrous Metals Society of China 20 (8) (2010) 1412–1417.
[59] Jui-Hsiang Lin, Wei-Hung Chen, Shih-Hsuan Su, Yuan-Kai Liao, Tse-Hao Ko, Journal of Power Sources 184 (1) (2008) 38–43.
[60] Yusuke Hiramitsu, Hitoshi Sato, Kenji Kobayashi, Michio Hori, Journal of Power Sources 196 (13) (2011) 5453–5469.
[61] H. Tawfik, Y. Hung, D. Mahajan, Journal of Power Sources 163 (2) (2007) 755–767.
[62] Moucheng Li, Suzhen Luo, Chaoliu Zeng, Jianian Shen, Haichao Lin, Chunan Cao, Corrosion Science 46 (6) (2004) 1369–1380.
[63] Ji Hun Park, Dongjin Byun, Joong Kee Lee, Materials Chemistry and Physics 128 (1–2) (2011) 39–43.
[64] E.A. Cho, U.-S. Jeon, S.-A. Hong, I.-H. Oh, S.-G. Kang, Journal of Power Sources 142 (1–2) (2005) 177–183.
[65] Y.J. Ren, C.L. Zeng, Journal of Power Sources 182 (2) (2008) 524–530.
[66] Young-Hoon Yun, International Journal of Hydrogen Energy 35 (4) (2010) 1713–1718.
[67] M.F. Mathias, R. Makharia, H.A. Gasteiger, J.J. Conley, T.J. Fuller, G.J. Gittleman, S.S. Kocha, D.P. Miller, C.K. Mittelsteadt, T. Xie, S.G. Yan, P.T. Yu, The Electrochemical Society Interface 14 (3) (2005) 24–35.
[68] Wu Bi, Qunhui Sun, Yulin Deng, Thomas F. Fuller, Electrochimica Acta 54 (6) (2009) 1826–1833.
[69] D.A. Stevens, M.T. Hicks, G.M. Haugen, J.R. Dahn, Journal of The Electrochemical Society 152 (12) (2005) A2309–A2315.
[70] N. Yousfi-Steiner, Ph. Moçotéguy, D. Candusso, D. Hissel, Journal of Power Sources 194 (1) (2009) 130–145.
[71] Shengsheng Zhang, Xiao-Zi Yuan, Jason Ng Cheng Hin, Haijiang Wang, Jinfeng Wu, K. Andreas Friedrich, Mathias Schulze, Journal of Power Sources 195 (4) (2010) 1142–1148.
[72] Minoru Inaba, Masashi Sugishita, Junpei Wada, Koichi Matsuzawa, Hirohisa Yamada, Akimasa Tasaka, Journal of Power Sources 178 (2) (2008) 699–705.
[73] Ting-Chu Jao, Guo-Bin Jung, Pei-Hung Chi, Shih-Tsung Ke, Shih-Hung Chan, Journal of Power Sources 196 (4) (2011) 1818–1825.
[74] Karachakorn Panha, Michael Fowler, Xiao-Zi Yuan, Haijiang Wang, Applied Energy 93 (2012) 90–97.
[75] G.J.M. Janssen, E.F. Sitters, A. Pfrang, Journal of Power Sources 191 (2) (2009) 501–509.
[76] Maji Luo, Chengyong Huang, Wei Liu, Zhiping Luo, Mu Pan, International Journal of Hydrogen Energy 35 (7) (2010) 2986–2993.
[77] Rod Borup, Jeremy Meyers, Bryan Pivovar, Yu Seung Kim, Rangachary Mukundan, Nancy Garland, Deborah Myers, Mahlon Wilson, Fernando Garzon, David Wood, Piotr Zelenay, Karren More, Ken Stroh, Tom Zawodzinski, James Boncella, James E. McGrath, Minoru Inaba, Kenji Miyatake, Michio Hori, Kenichiro Ota, Zempachi Ogumi, Seizo Miyata, Atsushi Nishikata, Zyun Siroma, Yoshiharu Uchimoto, Kazuaki Yasuda, Ken-ichi Kimijima, Norio Iwashita, Chemical Reviews 107 (10) (2007) 3904–3951.
[78] Hiroshi Ito, Tetsuhiko Maeda, Akihiro Nakano, Hiroyasu Takenaka, International Journal of Hydrogen Energy 36 (17) (2011) 10527–10540.
[79] J. Larminie, A. Dicks, Fuel Cell Systems Explained, second ed., John Wiley & Sons Ltd., 2003, pp. 70–71.
[80] Aidan Li, Siew Hwa Chan, Nam-trung Nguyen, Electrochemistry Communications 11 (4) (2009) 897–900.
[81] Wen-Kai Chao, Chih-Ming Lee, Du-Cheng Tsai, Chih-Cheng Chou, Kan-Lin Hsueh, Fuh-Sheng Shieu, Journal of Power Sources 185 (1) (2008) 136–142.
[82] Zhili Miao, Hongmei Yu, Wei Song, Dan Zhao, Lixing Hao, Baolian Yi, Zhigang Shao, Electrochemistry Communications 11 (4) (2009) 787–790.
[83] Un Ho Jung, Ki Tae Park, Eun Hee Park, Sung Hyun Kim, Journal of Power Sources 159 (1) (2006) 529–532.
[84] Singaram Vengatesan, Hyoung-Juhn Kim, Sang-Yeop Lee, EunAe Cho, Heung Yong Ha, In-Hwan Oh, Seong-Ahn Hong, Tae-Hoon Lim, International Journal of Hydrogen Energy 33 (1) (2008) 171–178.
[85] Hua-Neng Su, Li-Jun Yang, Shi-Jun Liao, Qiao Zeng, Electrochimica Acta 55 (28) (2010) 8894–8900.
[86] Ahmet Turhan, Soowhan Kim, Marta Hatzell, Matthew M. Mench, Electrochimica Acta 55 (8) (2010) 2734–2745.
[87] Jin Hyun Nam, Kyu-Jin Lee, Gi-Suk Hwang, Charn-Jung Kim, Massoud Kaviany, International Journal of Heat and Mass Transfer 52 (11–12) (2009) 2779–2791.
[88] Tak Cheung Yau, Massimiliano Cimenti, Xiaotao Bi, Jürgen Stumper, Journal of Power Sources 196 (22) (2011) 9437–9444.
[89] Zijie Lu, Michael M. Daino, Cody Rath, Satish G. Kandlikar, International Journal of Hydrogen Energy 35 (9) (2010) 4222–4233.
[90] Wei-Mon Yan, Dong-Kai Wu, Xiao-Dong Wang, Ai-Lien Ong, Duu-Jong Lee, Ay Su, Journal of Power Sources 195 (17) (2010) 5731–5734.
[91] Wei Dai, Haijiang Wang, Xiao-Zi Yuan, Jonathan Martin, Jun Shen, Mu Pan, Zhiping Luo, Journal of Power Sources 188 (1) (2009) 122–126.
[92] M.S. Ismail, T. Damjanovic, D.B. Ingham, L. Ma, M. Pourkashanian, Journal of Power Sources 195 (19) (2010) 6619–6628.
[93] Minjeh Ahn, Yong-Hun Cho, Yoon-Hwan Cho, Jinho Kim, Namgee Jung, Yung-Eun Sung, Electrochimica Acta 56 (5) (2011) 2450–2457.
[94] Xiaoli Wang, Huamin Zhang, Jianlu Zhang, Haifeng Xu, Xiaobing Zhu, Jian Chen, Baolian Yi, Journal of Power Sources 162 (1) (2006) 474–479.
[95] Jacob M. LaManna, Satish G. Kandlikar, International Journal of Hydrogen Energy 36 (8) (2011) 5021–5029.
[96] Chung-Jen Tseng, Shih-Kun Lo, Energy Conversion and Management 51 (4) (2010) 677–684.
[97] F.E. Hizir, S.O. Ural, E.C. Kumbur, M.M. Mench, Journal of Power Sources 195 (11) (2010) 3463–3471.
[98] Tatsumi Kitahara, Toshiaki Konomi, Hironori Nakajima, Journal of Power Sources 195 (8) (2010) 2202–2211.
[99] Zhigang Zhan, Jinsheng Xiao, Dayong Li, Mu Pan, Runzhang Yuan, Journal of Power Sources 160 (2) (2006) 1041–1048.
[100] Haolin Tang, Shenlong Wang, Mu Pan, Runzhang Yuan, Journal of Power Sources 166 (1) (2007) 41–46.
[101] Jeong Hwan Chun, Ki Tae Park, Dong Hyun Jo, Ji Young Lee, Sang Gon Kim, Sun Hee Park, Eun Sook Lee, Jy-Young Jyoung, Sung Hyun Kim, International Journal of Hydrogen Energy 36 (14) (2011) 8422–8428.
[102] Irfan S. Hussaini, Chao-Yang Wang, Journal of Power Sources 187 (2) (2009) 444–451.
[103] M.G. Santarelli, M.F. Torchio, Energy Conversion and Management 48 (1) (2007) 40–51.
[104] Kui Jiao, Jaewan Park, Xianguo Li., Applied Energy 87 (9) (2010) 2770–2777.
[105] Wei Dai, Haijiang Wang, Xiao Zi Yuan, Jonathan J. Martin, Zhiping Luo, Mu Pan, Journal of Power Sources 185 (2) (2008) 1267–1271.
[106] T. Ous, C. Arcoumanis, Journal of Power Sources 187 (1) (2009) 182–189.
[107] Mehdi Amirinejad, Soosan Rowshanzamir, Mohammad H. Eikani, Journal of Power Sources 161 (2) (2006) 872–875.
[108] Jianlu Zhang, Zhong Xie, Jiujun Zhang, Yanghua Tang, Chaojie Song, Titichai Navessin, Zhiqing Shi, Datong Song, Haijiang Wang, David P. Wilkinson, Zhong-Sheng Liu, Steven Holdcroft, Journal of Power Sources 160 (2) (2006) 872–891.
[109] Jin-Cherng Shyu, Kan-Lin Hsueh, Fanghei Tsau, Energy Conversion and Management 52 (12) (2011) 3415–3424.
[110] Saswata Bose, Tapas Kuila, Thi Xuan Hien Nguyen, Nam Hoon Kim, Kin-tak Lau, Joong Hee Lee, Progress in Polymer Science 36 (6) (2011) 813–843.
[111] Eiji Endoh, Hisao Kawazoe, Hideki Nakagawa, Electrochemical Society Transactions 1 (8) (2006) 221–227.
[112] Qingting Liu, Xujin Bao, Daniel M. Rogers, Siqin Zou, Electrochemical Society Transactions 30 (1) (2011) 25–32.
[113] Sang-Young Lee, Gunter Scharfenberger, Wolfgang H. Meyer, Gerhard Wegner, Journal of Power Sources 163 (1) (2006) 27–33.
[114] Zhongwei Chen, Ryan Hsu, Electrochemical Society Transactions 25 (1) (2009) 1151–1157.
[115] Bruno R. Matos, Elisabete I. Santiago, Fabio C. Fonseca, Marcelo Linardi, Vladimir Lavayen, Rodrigo G. Lacerda, Luiz O. Ladeira, Andre S. Ferlauto, Journal of The Electrochemical Society 154 (12) (2007) B1358–B1361.
[116] Mathieu Martinez, Cristina Iojoiu, Patrick Judeinstein, L. Cointeaux, Jean-Claude Lepretre, Jean-Yves Sanchez, Electrochemical Society Transactions 25 (1) (2009) 1647–1657.
[117] Eiji Endoh, Electrochemical Society Transactions 16 (2) (2008) 1229–1240.
[118] Elisabete I. Santiago, Bruno R. Matos, Fabio C. Fonseca, Marcelo Linardi, Electrochemical Society Transactions 11 (1) (2007) 151–157.
[119] H. Nakajima, S. Nomura, T. Sugimoto, S. Nishikawa, I. Honma, Journal of The Electrochemical Society 149 (8) (2002) A953–A959.
[120] Kui Jiao, Xianguo Li, Progress in Energy and Combustion Science 37 (3) (2011) 221–291.
[121] Yuka Oono, Takashi Fukuda, Atsuo Sounai, Michio Hori, Journal of Power Sources 195 (4) (2010) 1007–1014.
[122] Gang Liu, Huamin Zhang, Jingwei Hu, Yunfeng Zhai, Dongyan Xu, Zhigang Shao, Journal of Power Sources 162 (1) (2006) 547–552.
[123] Qingfeng Li, Jens Oluf Jensen, Robert F. Savinell, Niels J. Bjerrum, Progress in Polymer Science 34 (5) (2009) 449–477.
[124] A. Bazylak, D. Sinton, Z.-S. Liu, N. Djilali, Journal of Power Sources 163 (2) (2007) 784–792.
[125] H.M. Yu, J.O. Schumacher, M. Zobel, C. Hebling, Journal of Power Sources 145 (2) (2005) 216–222.
[126] Takashi Sasabe, Shohji Tsushima, Shuichiro Hirai, International Journal of Hydrogen Energy 35 (20) (2010) 11119–11128.
[127] H. Markötter, I. Manke, Ph. Krüger, T. Arlt, J. Haussmann, M. Klages, H. Riesemeier, Ch. Hartnig, J. Scholta, J. Banhart, Electrochemistry Communications 13 (9) (2011) 1001–1004.
[128] Yoshio Utaka, Ikunori Hirose, Yutaka Tasaki, International Journal of Hydrogen Energy 36 (15) (2011) 9128–9138.
[129] Phengxay Deevanhxay, Takashi Sasabe, Shohji Tsushima, Shuichiro Hira, International Journal of Hydrogen Energy 36 (17) (2011) 10901–10907.
[130] Takashi Sasabe, Phengxay Deevanhxay, Shohji Tsushima, Shuichiro Hirai, Journal of Power Sources 196 (20) (2011) 8197–8206.

[131] Christoph Hartnig, Ingo Manke, Robert Kuhn, Sebastian Kleinau, Jürgen Goebbels, John Banhart, Journal of Power Sources 188 (2) (2009) 468–474.
[132] Takashi Sasabe, Phengxay Deevanhxay, Shohji Tsushima, Shuichiro Hirai, Electrochemistry Communications 13 (6) (2011) 638–641.
[133] Ph. Krüger, H. Markötter, J. Haußmann, M. Klages, T. Arlt, J. Banhart, Ch. Hartnig, I. Manke, J. Scholta, Journal of Power Sources 196 (12) (2011) 5250–5255.
[134] C. Hartnig, I. Manke, Encyclopedia of Electrochemical Power Sources (2009) 738–757.
[135] J. Park, Xianguo Li, D. Tran, T. Abdel-Baset, D.S. Hussey, D.L. Jacobson, M. Arif, International Journal of Hydrogen Energy 33 (13) (2008) 3373–3384.
[136] J.P. Owejan, T.A. Trabold, D.L. Jacobson, D.R. Baker, D.S. Hussey, M. Arif, International Journal of Heat and Mass Transfer 49 (25–26) (2006) 4721–4731.
[137] Mingtao Wang, Kirk W. Feindel, Steven H. Bergens, Roderick E. Wasylishen, Journal of Power Sources 195 (21) (2010) 7316–7322.
[138] Jacqueline M. Sergi, Satish G. Kandlikar, International Journal of Hydrogen Energy 36 (19) (2011) 12381–12392.
[139] T. Ous, C. Arcoumanis, Journal of Power Sources 173 (1) (2007) 137–148.
[140] Talal Ous, C. Arcoumanis, International Journal of Hydrogen Energy 34 (8) (2009) 3476–3487.
[141] F.Y. Zhang, X.G. Yang, C.Y. Wang, Journal of The Electrochemical Society 153 (2) (2006) A225–A232.
[142] Zhigang Zhan, Chen Wang, Weiguo Fu, Mu Pan, International Journal of Hydrogen Energy 37 (1) (2012) 1094–1105.
[143] A. Bazylak, International Journal of Hydrogen Energy 34 (9) (2009) 3845–3857.
[144] Shohji Tsushima, Shuichiro Hirai, Progress in Energy and Combustion Science 37 (2) (2011) 204–220.
[145] N. Djilali, Energy 32 (2007) 269–280.
[146] Serhat Yesilyurmt, Journal of Fuel Cell Science and Technology 7 (3) (2010) 031008–031017.
[147] K.D. Kreuer, S.J. Paddison, E. Spohr, M. Schuster, Chemical Reviews 104 (2004) 4637–4678.
[148] Jin Hyun Nam, Massoud Kaviany, International Journal of Heat and Mass Transfer 46 (24) (2003) 4595–4611.
[149] K. Seidenberger, F. Wilhelm, T. Schmitt, W. Lehnert, J. Scholta, Journal of Power Sources 196 (12) (2011) 5317–5324.
[150] J.E. Dawes, N.S. Hanspal, O.A. Family, A. Turan, Chemical Engineering Science 64 (12) (2009) 2781–2794.
[151] Yun Wang, Suman Basu, Chao-Yang Wang, Journal of Power Sources 179 (2) (2008) 603–617.
[152] Stefano Cordiner, Simon Pietro Lanzani, Vincenzo Mulone, International Journal of Hydrogen Energy 36 (16) (2011) 10366–10375.
[153] Angelo Esposito, Cesare Pianese, Yann G. Guezennec, Journal of Power Sources 195 (13) (2010) 4149–4159.
[154] Hua Meng, International Journal of Hydrogen Energy 34 (13) (2009) 5488–5497.
[155] Hua Meng, International Journal of Hydrogen Energy 35 (11) (2010) 5569–5579.
[156] Z. Lu, S.G. Kandlikar, C. Rath, M. Grimm, W. Domigan, A.D. White, M. Hardbarger, J.P. Owejan, T.A. Trabold, International Journal of Hydrogen Energy 34 (8) (2009) 3445–3456.
[157] Xun Zhu, P.C. Sui, Ned Djilali, Journal of Power Sources 172 (1) (2007) 287–295.
[158] Anh Dinh Le, Biao Zhou, Huan-Ruei Shiu, Chun-I. Lee, Wen-Chen Chang, Journal of Power Sources 195 (21, 1) (2010) 7302–7315.
[159] A. Theodorakakos, T. Ous, M. Gavaises, J.M. Nouri, N. Nikolopoulos, H. Yanagihara, Journal of Colloid and Interface Science 300 (2) (2006) 673–687.
[160] J. Zachary Fishman, Hilary Leung, A. Bazylak, International Journal of Hydrogen Energy 35 (17) (2010) 9144–9150.
[161] Jon P. Owejan, Jeffrey J. Gagliardo, Jacqueline M. Sergi, Satish G. Kandlikar, Thomas A. Trabold, International Journal of Hydrogen Energy 34 (8) (2009) 3436–3444.
[162] Xianguo Li, Imran Sabir, International Journal of Hydrogen Energy 30 (4) (2005) 359–371.
[163] Xiao-Guang Yang, Qiang Ye, Ping Cheng, International Journal of Hydrogen Energy 36 (19) (2011) 12524–12537.
[164] J.J. Hwnag, W.R. Chang, R.G. Peng, P.Y. Chen, A. Su, International Journal of Hydrogen Energy 33 (20) (2008) 5718–5727.
[165] Daniel G. Strickland, Shawn Litster, Juan G. Santiago, Journal of Power Sources 174 (1) (2007) 272–281.
[166] Hong Sun, Guangsheng Zhang, Lie-Jin Guo, Hongtan Liu, Journal of Power Sources 158 (1) (2006) 326–332.
[167] Alex Hakenjos, Harald Muenter, Ursula Wittstadt, Christopher Hebling, Journal of Power Sources 131 (1–2) (2004) 213–216.
[168] Shou-Shing Hsieh, Bing-Shyan Her, Yi-Ji Huang, Energy Conversion and Management 52 (2) (2011) 975–982.
[169] Andrew Higier, Hongtan Liu, Journal of Power Sources 193 (2) (2009) 639–648.
[170] Guangsheng Zhang, Liejin Guo, Bin Ma, Hongtan Liu, Journal of Power Sources 188 (1) (2009) 213–219.
[171] Jürgen Stumper, Stephen A. Campbell, David P. Wilkinson, Mark C. Johnson, Mike Davis, Electrochimica Acta 43 (24) (1998) 3773–3783.
[172] Hui Li, Yanghua Tang, Zhenwei Wang, Zheng Shi, Shaohong Wu, Datong Song, Jianlu Zhang, Khalid Fatih, Jiujun Zhang, Haijiang Wang, Zhongsheng Liu, Rami Abouatallah, Antonio Mazza, Journal of Power Sources 178 (1) (2008) 103–117.
[173] Dusan Spernjak, Ajay K. Prasad, Suresh G. Advani, Journal of Power Sources 170 (2) (2007) 334–344.
[174] F. Barreras, A. Lozano, L. Valiño, C. Marín, A. Pascau, Journal of Power Sources 144 (1) (2005) 54–66.
[175] W. Goddard, B. Merinov, A. Vanduin, T. Jacob, M. Blanco, V. Molinero, S.S. Jang, Y.H. Jang, Molecular Simulation 32 (3–4) (2006) 251–268.
[176] M. Teliska, W.E. O'Grady, D.E. Ramaker, The Journal of Physical Chemistry B 109 (16) (2005) 8076–8084.
[177] Z.D. Wei, H.B. Ran, X.A. Liu, Y. Liu, C.X. Sun, S.H. Chan, P.K. Shen, Electrochimica Acta 51 (15) (2006) 3091–3096.
[178] Y. Shao-Horn, W.C. Sheng, S. Chen, P.J. Ferreira, E.F. Holby, D. Morgan, Chemistry and Materials Science 46 (3–4) (2007) 285–305.
[179] Wu Bi, Thomas F. Fuller, Journal of Power Sources 178 (1) (2008) 188–196.
[180] Xuan Cheng, Ling Chen, Cheng Peng, Zhiwu Chen, Ying Zhang, Qinbai Fan, Journal of The Electrochemical Society 151 (1) (2004) A48–A52.
[181] F.H. Garzon, John Davey, Rodney Borup, Electrochemical Society Transactions 1 (8) (2006) 153–166.
[182] Shuo Chen, Hubert A. Gasteiger, Katsuichiro Hayakawa, Tomoyuki Tada, Yang Shao-Horn, Journal of The Electrochemical Society 157 (1) (2010) A82–A97.
[183] C.H. Paik, G.S. Saloka, G.W. Graham, Electrochemical and Solid-State Letters 10 (2) (2007) B39–B42.
[184] Masanobu Uchimura, Shyam S. Kocha, Electrochemical Society Transactions 11 (1) (2007) 1215–1226.
[185] Wu Bi, Gary E. Gray, Thomas F. Fuller, Electrochemical and Solid-State Letters 10 (5) (2007) B101–B104.
[186] Ronald S. Goeke, Abhaya K. Datye, Plamen Atanassov, Jean St-Pierre, Electrochemical Society Transactions 33 (1) (2010) 361–368.
[187] Sarah C. Ball, Sarah L. Hudson, Brian Theobald, David Thompsett, Electrochemical Society Transactions 3 (1) (2006) 595–605.
[188] Sarah C. Ball, Sarah L. Hudson, Brian R. Theobald, David Thompsett, Electrochemical Society Transactions 11 (1) (2007) 1267–1278.
[189] Ping Yu, Marianne Pemberton, Paul Plasse, Journal of Power Sources 144 (1) (2005) 11–20.
[190] Bruno Pollet, Jill E. Newton, Jon A. Preece, Oliver J. Curnick, Electrochemical Society Transactions 41 (1) (2011) 2165–2173.
[191] Mahlon S. Wilson, Fernando H. Garzon, Kurt E. Sickafus, Shimshon Gottesfeld, Journal of The Electrochemical Society 140 (10) (1993) 2872–2877.
[192] Jian Xie, David L. Wood, Karren L. More, Plamen Atanassov, Rodney L. Borup, Journal of The Electrochemical Society 152 (5) (2005) A1011–A1020.
[193] Karl J.J. Mayrhofer, Josef C. Meier, Sean J. Ashton, Gustav K.H. Wiberg, Florian Kraus, Marianne Hanzlik, Matthias Arenz, Electrochemistry Communications 10 (8) (2008) 1144–1147.
[194] Timothy W. Patterson, Robert M. Darling, Electrochemical and Solid-State Letters 9 (4) (2006) A183–A185.
[195] Z.Y. Liu, B.K. Brady, R.N. Carter, B. Litteer, M. Budinski, J.K. Hyun, D.A. Muller, Journal of The Electrochemical Society 155 (10) (2008) B979–B984.
[196] Jingxin Zhang, Brian A. Litteer, Wenbin Gu, Han Liu, Hubert A. Gasteiger, Journal of The Electrochemical Society 154 (10) (2007) B1006–B1011.
[197] A.P. Young, J. Stumper, S. Knights, E. Gyenge, Journal of The Electrochemical Society 157 (3) (2010) B425–B436.
[198] Carlotta Francia, Vijaykumar S. Ijeri, Stefania Specchia, Paolo Spinelli, Journal of Power Sources 196 (4) (2011) 1833–1839.
[199] Sumit Kundu, Michael W. Fowler, Leonardo C. Simon, Rami Abouatallah, Natasha Beydokhti, Journal of Power Sources 183 (2) (2008) 619–628.
[200] Sumit Kundu, Michael W. Fowler, Leonardo C. Simon, Rami Abouatallah, Natasha Beydokhti, Journal of Power Sources 195 (21) (2010) 7323–7331.
[201] Y. Kawasoe, S. Tanaka, T. Kuroki, H. Kusaba, K. Ito, Y. Teraoka, K. Sasaki, Journal of The Electrochemical Society 154 (9) (2007) B969–B975.
[202] Sarah C. Ball, Brian Theobald, David Thompsett, Sarah Hudson, Electrochemical Society Transactions 1 (8) (2006) 141–152.
[203] Tomoyuki Tada, Yumi Yamamoto, Koichi Matsutani, Katsuichiro Hayakawa, Tatsunori Namai, Electrochemical Society Transactions 16 (2) (2008) 215–224.
[204] Sang Hyun Ahn, Soo-Kil Kim, Oh Joong Kwon, Sun-Mi Hwang, Jae Jeong Kim, Electrochemical Society Transactions 16 (2) (2008) 1111–1116.
[205] Margaret A. Gabriel, Thierry Deutsch, Alejandro A. Franco, Electrochemical Society Transactions 25 (22) (2010) 1–6.
[206] Jiajun Wang, Geping Yin, Yuyan Shao, Zhenbo Wang, Yunzhi Gao, Journal of The Electrochemical Society 154 (7) (2007) B687–B693.
[207] Zhongwei Chen, Weiqiao Deng, Xin Wang, Yushan Yan, Electrochemical Society Transactions 11 (1) (2007) 1289–1299.
[208] Zhe Tang, How Y. Ng, Jianyi Lin, Andrew T.S. Wee, Daniel H.C. Chua, Journal of The Electrochemical Society 157 (2) (2010) B245–B250.
[209] Wei Zhu, Jim P. Zheng, R. Liang, Ben Wang, Chun Zhang, Shawn Walsh, George Au, Edward J. Plichta, Electrochemical Society Transactions 16 (2) (2008) 1615–1626.
[210] W. Zhu, J.P. Zheng, R. Liang, B. Wang, C. Zhang, G. Au, E.J. Plichta, Journal of The Electrochemical Society 156 (9) (2009) B1099–B1105.
[211] R. Imran Jafri, T. Arockiados, N. Rajalakshmi, S. Ramaprabhu, Journal of The Electrochemical Society 157 (6) (2010) B874–B879.

[212] Anil V. Virkar, Yingke Zhou, Journal of The Electrochemical Society 154 (6) (2007) B540–B547.
[213] Dong-Ha Lim, Woo-Jin Lee, Jess Wheldon, Nathan L. Macy, William H. Smyrl, Journal of The Electrochemical Society 157 (6) (2010) B862–B867.
[214] Yuichi Suzuki, Akimitsu Ishihara, Shigenori Mitsushima, Nobuyuki Kamiya, Ken-ichiro Ota, Electrochemical and Solid-State Letters 10 (7) (2007) B105–B107.
[215] Madhu Sudan Saha, Ruying Li, Mei Cai, Xueliang Sun, Electrochemical and Solid-State Letters 10 (8) (2007) B110–B113.
[216] Zhongwei Chen, Mahesh Waje, Wenzhen Li, Yushan Yan, Electrochemical Society Transactions 11 (1) (2007) 1301–1311.
[217] Wolfgang Schmittinger, Ardalan Vahidi, Journal of Power Sources 180 (1) (2008) 1–14.
[218] N. Yousfi-Steiner, Ph. Moçotéguy, D. Candusso, D. Hissel, A. Hernandez, A. Aslanides, Journal of Power Sources 183 (1) (2008) 260–274.
[219] J. Parrondo, M. Ortueta, F. Mijangos, Brazilian Journal of Chemical Engineering 24 (03) (2007) 411–419.
[220] Ahmet Kusoglu, Brian L. Kienitz, Adam Z. Weber, Journal of The Electrochemical Society 158 (12) (2011) B1504–B1514.
[221] Vivek S. Murthi, Joseph Dura, Sushil Satija, Charles Majkrzak, Electrochemical Society Transactions 16 (2) (2008) 1471–1485.
[222] M.B. Statterfield, P.W. Majsztrik, H. Ota, J.B. Benziger, A.B. Bocarsly, Journal of Polymer Science Part B: Polymer Physics 44 (16) (2006) 2327–2345.
[223] Paul W. Majsztrik, Andrew B. Bocarsly, Jay B. Benziger, Macromolecules 41 (24) (2008) 9849–9862.
[224] Ahmet Kusoglu, Anette M. Karlsson, Michael H. Santare, Simon Cleghorn, William B. Johnson, Journal of Power Sources 161 (2) (2006) 987–996.
[225] Ahmet Kusoglu, Michael H. Santare, Anette M. Karlsson, Simon Cleghorn, William B. Johnson, Journal of The Electrochemical Society 157 (5) (2010) B705–B713.
[226] Timothy J. Silverman, Jeremy P. Meyers, Joseph J. Beaman, Journal of The Electrochemical Society 157 (10) (2010) B1376–B1381.
[227] Xiqiang Yan, Ming Hou, Liyan Sun, Haibo Cheng, Youlu Hong, Dong Liang, Qiang Shen, Pingwen Ming, Baolian Yi, Journal of Power Sources 163 (2) (2007) 966–970.
[228] Vijay A. Sethuraman, John W. Weidner, Andrew T. Haug, Lesia V. Protsailo, Journal of The Electrochemical Society 155 (2) (2008) B119–B124.
[229] D.A. Schiraldi, Journal of Macromolecular Science, Part C: Polymer Reviews 46 (3) (2006) 315–327.
[230] Jingrong Yu, Toyoaki Matsuura, Yusuke Yoshikawa, Md Nazrul Islam, Michio Hori, Journal of Physical Chemistry Chemical Physics (7) (2005) 373–378.
[231] Cheng Chen, Thomas F. Fuller, Polymer Degradation and Stability 94 (9) (2009) 1436–1447.
[232] H.A. Gasteiger, W. Gu, B. Litteer, R. Makharia, B. Brady, M. Budinski, E. Thompson, F.T. Wagner, S.G. Yan, P.T. Yu, Catalyst Degradation Mechanisms in PEM and Direct Methanol Fuel Cells, in: Mini-micro Fuel Cells; NATO Science for Peace and Security Series C: Environmental Security, 2008, pp. 225–233, http://dx.doi.org/10.1007/978-1-4020-8295-5_15.
[233] X.Y. Huang, R. Solasi, Y. Zou, M. Feshler, K. Reifsnider, D. Condit, S. Burlatsky, T. Madden, Journal of Polymer Science Part B: Polymer Physics 44 (16) (2006) 2346–2357.
[234] A. Reyna-Valencia, S. Kaliguine, M. Bousmina, Journal of Applied Polymer Science 98 (6) (2005) 2380–2393.
[235] Ahmet Kusoglu, Michael H. Santare, Anette M. Karlsson, Journal of Polymer Science Part B: Polymer Physics 49 (21) (2011) 1506–1517.
[236] Ahmet Kusoglu, Anette M. Karlsson, Michael H. Santare, Simon Cleghorn, William B. Johnson, Journal of Power Sources 170 (2) (2007) 345–358.
[237] Vijay A. Sethuraman, John W. Weidner, Andrew T. Haug, Sathya Motupally, Lesia V. Protsailo, Journal of The Electrochemical Society 155 (1) (2008) B50–B57.
[238] Eiji Endoh, Shinji Terazono, Hardiyanto Widjaja, Yasuyuki Takimoto, Electrochemical and Solid-State Letters 7 (7) (2004) A209–A211.
[239] Amanda Collier, Haijiang Wang, Xiao Zi Yuan, Jiujun Zhang, David P. Wilkinson, International Journal of Hydrogen Energy 31 (13) (2006) 1838–1854.
[240] Carl A. Reiser, Lawrence Bregoli, Timothy W. Patterson, Jung S. Yi, J. Deliang Yang, Mike L. Perry, Thomas D. Jarvi, Electrochemical and Solid-State Letters 8 (6) (2005) A273–A276.
[241] Masanobu Uchimura, Seiho Sugawara, Yosuke Suzuki, Jianbo Zhang, Shyam S. Kocha, Electrochemical Society Transactions 16 (2) (2008) 225–234.
[242] Wolfgang R.R. Baumgartner, Wolfgang R.R. Baumgartner, Eva Wallnöfer, Thomas Schaffer, Viktor Hacker, Volker Peinecke, Peter Prenninger, Electrochemical Society Transactions 3 (1) (2006) 811–825.
[243] Yuyan Shao, Jun Wang, Rong Kou, Mark Engelhard, Jun Liu, Yong Wang, Yuehe Lin, Electrochimica Acta 54 (11) (2009) 3109–3114.
[244] S. Maass, F. Finsterwalder, G. Frank, R. Hartmann, C. Merten, Journal of Power Sources 176 (2) (2008) 444–451.
[245] Wei Li, Alan M. Lane, Electrochimica Acta 55 (22) (2010) 6926–6931.
[246] A.P. Young, J. Stumper, E. Gyenge, Journal of The Electrochemical Society 156 (8) (2009) B913–B922.
[247] K.H. Kangasniemi, D.A. Condit, T.D. Jarvi, Journal of The Electrochemical Society 151 (4) (2004) E125–E132.
[248] Renato A. Antunes, Mara Cristina L. Oliveira, Gerhard Ett, Volkmar Ett, International Journal of Hydrogen Energy 35 (8) (2010) 3632–3647.
[249] Kung-Hsu Hou, Chien-Hung Lin, Ming-Der Ger, Sheau-Wen Shiah, Hsi-Ming Chou, International Journal of Hydrogen Energy 37 (4) (2012) 3890–3896.
[250] Ying Yang, Lie-jin Guo, Hongtan Liu, International Journal of Hydrogen Energy 36 (2) (2011) 1654–1663.
[251] Heli Wang, Mary Ann Sweikart, John A. Turner, Journal of Power Sources 115 (2) (2003) 243–251.
[252] Heli Wang, John A. Turner, Journal of Power Sources 128 (2) (2004) 193–200.
[253] Johan André, Laurent Antoni, Jean-Pierre Petit, International Journal of Hydrogen Energy 35 (8) (2010) 3684–3697.
[254] Nada Zamel, Xianguo Li, Progress in Energy and Combustion Science 37 (3) (2011) 292–329.
[255] M. Kelly, Bernhard Egger, G. Fafilek, J. Besenhard, H. Kronberger, G. Nauer, Solid State Ionics 176 (25–28) (2005) 2111–2114.
[256] Y. Ishikawa, H. Hamada, M. Uehara, M. Shiozawa, Journal of Power Sources 179 (2) (2008) 547–552.
[257] Abdul-Kader Srouji, Matthew M. Mench, Polymer Electrolyte Fuel Cell Degradation (2012) 293–333.
[258] EunAe Cho, Jae-Joon Ko, Heung Yong Ha, Seong-Ahn Hong, Kwan-Young Lee, Tae-Won Lim, In-Hwan Oh, The Journal of The Electrochemical Society 150 (12) (2003) A1667–A1670.
[259] Dennis E. Curtin, Robert D. Lousenberg, Timothy J. Henry, Paul C. Tangeman, Monica E. Tisack, Journal of Power Sources 131 (1–2) (2004) 41–48.
[260] Qunhui Guo, Zhigang Qi, Journal of Power Sources 160 (2) (2006) 1269–1274.
[261] Jing Li, Stephen Lee, Joy Roberts, Electrochemical Society Transactions 11 (1) (2007) 595–605.
[262] Stephen Lee, Joy Roberts, Jing Li, Siyu Ye, Electrochemical Society Transactions 12 (1) (2008) 13–19.
[263] Shengsheng Zhang, Xiaozi Yuan, Haijiang Wang, Walter Mérida, Hong Zhu, Jun Shen, Shaohong Wu, Jiujun Zhang, International Journal of Hydrogen Energy 34 (1) (2009) 388–404.
[264] Qiangu Yan, Hossein Toghiani, Young-Whan Lee, Kaiwen Liang, Heath Causey, Journal of Power Sources 160 (2) (2006) 1242–1250.
[265] Shichun Mu, Pei Zhao, Cheng Xu, Ying Gao, Mu Pan, International Journal of Hydrogen Energy 35 (15) (2010) 8155–8160.
[266] Mathias Gerard, Jean-Philippe Poirot-Crouvezier, Daniel Hissel, Marie-Cécile Pera, International Journal of Hydrogen Energy 35 (22) (2010) 12295–12307.
[267] R. Alink, D. Gerteisen, M. Oszcipok, Journal of Power Sources 182 (1) (2008) 175–187.
[268] Feng Rong, Cheng Huang, Zhong-Sheng Liu, Datong Song, Qianpu Wang, Journal of Power Sources 175 (2) (2008) 699–711.
[269] Sang-Yeop Lee, Hyoung-Juhn Kim, EunAe Cho, Kug-Seung Lee, Tae-Hoon Lim, In Chul Hwang, Jong Hyun Jang, International Journal of Hydrogen Energy 35 (23) (2010) 12888–12896.
[270] Soowhan Kim, Manish Khandelwal, Charles Chacko, Matthew Mench, Electrochemical Society Transactions 16 (2) (2008) 1977–1986.
[271] X.G. Yang, Y. Tabuchi, F. Kagami, Chao-Yang Wang, Journal of The Electrochemical Society 155 (7) (2008) B752–B761.
[272] Suhao He, Matthew M. Mench, Journal of The Electrochemical Society 153 (9) (2006) A1724–A1731.
[273] Matthew Mench, Suhao He, Electrochemical Society Transactions 3 (1) (2006) 897–907.
[274] Shanhai Ge, Chao-Yang Wang, Journal of The Electrochemical Society 154 (12) (2007) B1399–B1406.
[275] Hiroshisa Yoshida, Yuka Miura, Journal of Membrane Science 68 (1–2) (1992) 1–10.
[276] Zijie Lu, Georgios Polizos, Digby D. Macdonald, E. Manias, Journal of The Electrochemical Society 155 (2) (2008) B163–B171.
[277] Shanhai Ge, Chao-Yang Wang, Electrochemical and Solid-State Letters 9 (11) (2006) A499–A503.
[278] Shanhai Ge, Chao-Yang Wang, Electrochimica Acta 52 (14) (2007) 4825–4835.
[279] Y. Ishikawa, T. Morita, K. Nakata, K. Yoshida, M. Shiozawa, Journal of Power Sources 163 (2) (2007) 708–712.
[280] Yuji Ishikawa, Tohru Morita, Keiichi Nakata, Kazuhiko Yoshida, Masahiro Shiozawa, Electrochemical Society Transactions 1 (6) (2006) 359–364.
[281] Morihiro Saito, Kikuko Hayamizu, Tatsuhiro Okada, The Journal of Physical Chemistry B 109 (8) (2005) 3112–3119.
[282] R. Mukundan, Yu Seung Kim, F.H. Garzon, Bryan Pivovar, Electrochemical Society Transactions 1 (8) (2006) 403–413.
[283] R.C. McDonald, C.K. Mittelsteadt, E.L. Thompson, Fuel Cells 4 (3) (2004) 208–213.
[284] Kevin G. Gallagher, Bryan S. Pivovar, Thomas F. Fuller, Journal of The Electrochemical Society 156 (3) (2009) B330–B338.
[285] Akihiko Koiwai, Atsushi Kamiya, Masaya Kawasumi, Electrochemical Society Transactions 11 (1) (2007) 587–593.
[286] Ahmet Kusoglu, Anette Karlsson, Michael Santare, Simon Cleghorn, William B. Johnson, Electrochemical Society Transactions 16 (2) (2008) 551–561.
[287] Hossein Ghassemi, Ram Subbaraman, Christopher Brockman, Brandon Pyle, Thomas Zawodzinski, Electrochemical Society Transactions 16 (2) (2008) 689–697.

[288] Jason B. Ballengee, Peter Pintauro, Electrochemical Society Transactions 41 (1) (2011) 1507–1516.
[289] Jinhui Pang, Haibo Zhang, Xuefeng Li, Dianfu Ren, Zhenhua Jiang, Macromolecular Rapid Communications 28 (24) (2007) 2332–2338.
[290] Z. Zhu, N.M. Walsby, H.M. Colquhoun, D. Thompsett, E. Petrucco, Fuel Cells 9 (4) (2009) 305–317.
[291] M.A. Navarra, A. Fernicola, S. Panero, B. Scrosati, Journal of The Electrochemical Society 153 (7) (2006) A1284–A1289.
[292] M.A. Navarra, S. Panero, B. Scrosati, Electrochemical and Solid-State Letters 8 (6) (2005) A324–A327.
[293] A. Martinelli, A. Matic, P. Jacobsson, L. Börjesson, M.A. Navarra, S. Panero, B. Scrosati, Journal of The Electrochemical Society 154 (8) (2007) G183–G187.
[294] Xin Wang, Wenzhen Li, Zhongwei Chen, Mahesh Waje, Yushan Yan, Journal of Power Sources 158 (1) (2006) 154–159.
[295] Sheng-Yang Huang, Prabhu Ganesan, Won Suk Jung, Nicholas Cadirov, Branko N. Popov, Electrochemical Society Transactions 33 (1) (2010) 483–491.
[296] Mike L. Perry, Timothy Patterson, Carl Reiser, Electrochemical Society Transactions 3 (1) (2006) 783–795.
[297] S. Vinod Selvaganesh, G. Selvarani, P. Sridhar, S. Pitchumani, A.K. Shukla, Journal of The Electrochemical Society 157 (7) (2010) B1000–B1007.
[298] Satheesh Sambandam, Vinodh Valluri, Wilaiwan Chanmanee, Normar De Tacconi, Wesley A. Wampler, Wen-Yuan Lin, Thomas F. Carlson, Vijay Ramani, Krishnan Rajeshwar, Journal of Chemical Science Vol. 121 (5) (2009) 655–664.
[299] H. Li, K. Lee, J. Zhang, Fundamentals and Applications, first ed., 2008, ISBN 978-1-84800-935-6, pp. 135–163.
[300] Madhusudhana R. Dowlapalli, Plamen Atanassov, Jian Xie, Gordon Rice, Electrochemical Society Transactions 1 (8) (2006) 41–50.
[301] Tatsuhiro Okada, Mikio Sugiura, Gang Xie, Electrochemical Society Transactions 3 (1) (2006) 667–676.
[302] J. Jayaraj, Y.C. Kim, K.B. Kim, H.K. Seok, E. Fleury, Science and Technology of Advanced Materials 6 (3–4) (2005) 282–289.
[303] Rujin Tian, Juncai Sun, International Journal of Hydrogen Energy 36 (11) (2011) 6788–6794.
[304] M.P. Brady, H. Wang, J.A. Turner, H.M. Meyer III, K.L. More, P.F. Tortorelli, B.D. McCarthy, Journal of Power Sources 195 (17) (2010) 5610–5618.
[305] Shine Joseph, J.C. McClure, P.J. Sebastian, J. Moreira, Edgar Valenzuela, Journal of Power Sources 177 (1) (2008) 161–166.
[306] Shuo-Jen Lee, Ching-Han Huang, Yu-Pang Chen, Journal of Materials Processing Technology 140 (1–3) (2003) 688–693.
[307] J. Wind, R. Späh, W. Kaiser, G. Böhm, Journal of Power Sources 105 (2) (2002) 256–260.
[308] Xuan Cheng, Zheng Shi, Nancy Glass, Lu Zhang, Jiujun Zhang, Datong Song, Zhong-Sheng Liu, Haijiang Wang, Jun Shen, Journal of Power Sources 165 (2) (2007) 739–756.
[309] Shucheng Sun, Hongmei Yu, Junbo Hou, Zhigang Shao, Baolian Yi, Pingwen Ming, Zho, Journal of Power Sources 177 (1) (2008) 137–141.
[310] Kui Jiao, Ibrahim E. Alaefour, Gholamreza Karimi, Xianguo Li, Electrochimica Acta 56 (8) (2011) 2967–2982.
[311] Junbo Hou, Hongmei Yu, Shengsheng Zhang, Shucheng Sun, Hongwei Wang, Baolian Yi, Pingwen Ming, Journal of Power Sources 162 (1) (2006) 513–520.
[312] Sang-Yeop Lee, Sang-Uk Kim, Hyoung-Juhn Kim, Jong Hyun Jang, In-Hwan Oh, Eun Ae Cho, Seong-Ahn Hong, Jaejun Ko, Tae-Won Lim, Kwan-Young Lee, Tae-Hoon Lim, Journal of Power Sources 180 (2) (2008) 784–790.
[313] G. Gavello, J. Zeng, C. Francia, U.A. Icardi, A. Graizzaro, S. Specchia, International Journal of Hydrogen Energy 36 (13) (2011) 8070–8081.
[314] Kah-Young Song, Hee-Tak Kim, International Journal of Hydrogen Energy 36 (19) (2011) 12417–12426.
[315] EunAe Cho, Jae-Joon Ko, Heung Yong Ha, Seong-Ahn Hong, Kwan-Young Lee, Tae-Won Lim, In-Hwan Oh, The Journal of The Electrochemical Society 151 (5) (2004) A661–A665.
[316] Liang Wang, Ajay K. Prasad, Suresh G. Advani, Journal of The Electrochemical Society 158 (12) (2011) B1499–B1503.
[317] Wei Song, Hongmei Yu, Lixing Hao, Baolian Yi, Zhigang Shao, International Journal of Hydrogen Energy 35 (20) (2010) 11129–11137.
[318] S. Roy, M.E. Orazem, Electrochemical Society Transactions 11 (1) (2007) 485–495.
[319] Ion C. Halalay, Swathy Swathirajan, Belabbes Merzougui, Michael P. Balogh, Gregory C. Garabedian, Michael K. Carpenter, Journal of The Electrochemical Society 158 (3) (2011) B313–B321.
[320] Jing Li, Ping He, Keping Wang, Mike Davis, Siyu Ye, Electrochemical Society Transactions 3 (1) (2006) 743–751.
[321] Keun-Hwan Oh, Wan-Keun Kim, Kyung A. Sung, Min-Ju Choo, Kwan-Woo Nam, Jang Wook Choi, Jung-Ki Park, International Journal of Hydrogen Energy 36 (21) (2011) 13695–13702.
[322] Guangyu Lin, Trung Van Nguyen, The Journal of The Electrochemical Society 152 (10) (2005) A1942–A1948.
[323] T. Colinart, S. Didierjean, O. Lottin, G. Maranzana, C. Moyne, Journal of The Electrochemical Society 155 (3) (2008) B244–B257.
[324] T. Colinart, A. Chenu, S. Didierjean, O. Lottin, S. Besse, Journal of Power Sources 190 (2) (2009) 230–240.
[325] G.S. Hwang, M. Kaviany, J.H. Nam, M.H. Kim, S.Y. Son, Journal of The Electrochemical Society 156 (2009) B1192.
[326] J. Ramousse, J. Deseure, O. Lottin, S. Didierjean, D. Maillet, Journal of Power Sources 145 (2) (2005) 416–427.
[327] N.P. Siegel, M.W. Ellis, D.J. Nelson, M.R. von Spakovsky, Journal of Power Sources 128 (2) (2004) 173–184.
[328] G.J.M. Janssen, M.L.J. Overvelde, Journal of Power Sources 101 (1) (2001) 117–125.
[329] Hiroyuki Uchida, Makoto Aoki, Masahiro Watanabe, Electrochemical Society Transactions 3 (1) (2006) 485–492.
[330] Wen Liu, S. Cleghorn, Electrochemical Society Transactions 1 (8) (2006) 263–273.
[331] Thor Anders Aarhaug, Ann Mari Svensson, Axel Baumann Ofstad, Jan Gregor Høydahl Sørli, Héloïse Couvert, Electrochemical Society Transactions 16 (2) (2008) 1687–1695.
[332] Jae Hong Kim, Yoo Yeon Jo, Eun Ae Cho, Jong Hyun Jang, Hyoung Juhn Kim, Tae-Hoon Lim, In-Hwan Oh, Jae Jun Ko, Ik Jae Son, Journal of The Electrochemical Society 157 (5) (2010) B633–B642.
[333] Gang Luo, Yan Ji, Chao-Yang Wang, Puneet K. Sinha, Electrochimica Acta 55 (19) (2010) 5332–5341.
[334] Yan Ji, Gang Luo, Chao-Yang Wang, Journal of The Electrochemical Society 157 (12) (2010) B1753–B1761.
[335] A. Casalegno, L. Colombo, S. Galbiati, R. Marchesi, Journal of Power Sources 195 (13) (2010) 4143–4148.
[336] Chaozhong Qin, Dirk Rensink, Stephan Fell, S. Majid Hassanizadeh, Journal of Power Sources 197 (2012) 136–144.
[337] M. Acosta, C. Merten, G. Eigenberger, H. Class, R. Helmig, B. Thoben, H. Müller-Steinhagen, Journal of Power Sources 159 (2) (2006) 1123–1141.
[338] J.P. Feser, A.K. Prasad, S.G. Advani, Journal of Power Sources 162 (2) (2006) 1226–1231.
[339] Guangli He, Pingwen Ming, Zongchang Zhao, Abuliti Abudula, Yu Xiao, Journal of Power Sources 163 (2) (2007) 864–873.
[340] Yun Wang, Sungchan Cho, Ralf Thiedmann, Volker Schmidt, Werner Lehnert, Xuhui Feng, International Journal of Heat and Mass Transfer 53 (5–6) (2010) 1128–1138.
[341] A. Casalegno, F. Bresciani, G. Groppi, R. Marchesi, Journal of Power Sources 196 (24) (2011) 10632–10639.
[342] Jeff T. Gostick, Marios A. Ioannidis, Michael W. Fowler, Mark D. Pritzker, Journal of Power Sources 173 (1) (2007) 277–290.
[343] Puneet K. Sinha, Chao-Yang Wang, Electrochimica Acta 52 (28) (2007) 7936–7945.
[344] A. Kopanidis, A. Theodorakakos, M. Gavaises, D. Bouris, International Journal of Thermal Sciences 50 (4) (2011) 456–467.
[345] Y. Ding, H.T. Bi, D.P. Wilkinson, Journal of Power Sources 196 (15) (2011) 6284–6292.
[346] Jürgen Becker, Christian Wieser, Stephan Fell, Konrad Steiner, International Journal of Heat and Mass Transfer 54 (7–8) (2011) 1360–1368.
[347] Tetsuya Koido, Toru Furusawa, Koji Moriyama, Journal of Power Sources 175 (1) (2008) 127–136.
[348] W.K. Liu, S.J.C. Cleghorn, B.E. Delaney, M. Crum, Chemical and Mechanical Membrane Degradation, in: Handbook of Fuel Cells: Fundamentals, Technology, and Applications. Advances in Electrocatalysis, Materials, Diagnostics and Durability, 2009, ISBN 978-0-470-72311-1. (Chapter 26).
[349] A. Pozio, R.F. Silva, M. De Francesco, L. Giorgi, Electrochimica Acta 48 (11) (2003) 1543–1549.
[350] Panagiotis Trogadas, Javier Parrondo, V. Ramani, Electrochemical Society Transactions 16 (2) (2008) 1725–1733.
[351] K.L. More, VII.I.2 Microstructural Characterization of Polymer Electrolyte Membrane Fuel Cell (PEMFC) Membrane Electrode Assemblies (MEAs), DOE Hydrogen Program FY 2005 Progress Report.
[352] K.L. More, IV.I.2 Microstructural Characterization of Polymer Electrolyte Membrane Fuel Cell (PEMFC) Membrane Electrode Assemblies (MEAs), DOE Hydrogen Program FY 2004 Progress Report.